Journal of Cleaner Production 501 (2025) 145254

Contents lists available at ScienceDirect

Journal of Cleaner Production

journal homepage: www.elsevier.com/locate/jclepro

Off-design performance of a hybrid renewable compressed air energy storage system: Dynamic simulation and thermo-economic analysis

Francesco Calise, Francesco Liberato Cappiello *, Luca Cimmino, Maria Vicidomini

DII - University of Naples Federico II, P.le Tecchio, 80 - 80125 Naples, Italy

ARTICLE INFO

Handling Editor: Liu Yu

Keywords:
Renewable energy systems
Advanced adiabatic compressed air energy storage
Co-simulation
Excess electricity
Electric energy storage system

ABSTRACT

This research proposes a novel co-simulation model for analyzing the time dependent performance of a compressed air energy storage (CAES) system driven by the renewable excess electricity. In particular, the system layout of the considered CAES includes: a compression train, an expansion train and a compressed air tank. All these components are modelled in MATLAB by suitable algorithms. The developed CAES is also coupled with a renewable plant supplying electricity to a plurality of users. The overall simulation model of the renewable plant, including the CAES, is developed in TRNSYS. The compressions train includes two centrifugal compressors and one reciprocating compressor. The expansion train includes three radial turbines. This model is designed for assessing the time dependent performance of the compressed air energy storage tracking the excess electricity in charging phase and the load in discharging phase. The models of the compressors and turbines are developed using the manufacturer maps approach. The selected user is a residential user including 50 buildings located in Naples, South of Italy. The proposed renewable plant consists of a compression train, featured by an overall capacity of 3.5 MW, a 1.5 MW expansion train and a 250 m^3 compressed air tank at 350 bar. This system is integrated with a 6.30 MW photovoltaic field and 2000 m^2 solar field of evacuated collectors. The photovoltaic electricity firstly meets the demand of the district users. The excess renewable electricity is used to drive the compressed air energy storage system. This system also includes a suitable waste heat management system, designed for storing the waste heat due to compression and reducing the air temperature at the inlet of each compressor. Such waste heat is used for heating the air delivered to the turbines. The thermal energy provided by the evacuated collector solar field is used for increasing the turbines inlet temperature.

The proposed system achieves promising energy results, being able to reduce by 59 % the primary energy demand of the selected residential district. Moreover, the compressed air energy storage system meets about 14 % of the district load. The proposed system shows a limited economic profitability with a payback period of 21 years, due to the high capital cost of the technologies involved in such plant.

1. Introduction

The integration of renewable-based technologies in the current energy systems is crucial for advancing the energy transition toward the decarbonization goals set for 2050 (Li et al., 2022a). In this framework, electricity storage systems (ESS) play a key role in the development of innovative renewable and smart energy networks (Calise et al., 2023a). ESSs are strategic for power security and to achieve a flexible and robust operation of power systems (Mehigan et al., 2022). Their massive utilization has been presently limited by their high capital costs (Calise et al., 2019a). Considering the expected massive electrification of user demands in all sectors (residential, transport and industrial) (Li et al., 2023), the future energy grids must be mandatory equipped with suitable energy storage systems to balance the phase shift between user demand and non-programmable renewable electricity production (mainly wind and solar). This is crucial to limit energy transportation and exchange among the different local grids (Zhu et al., 2022). Consequently, ESSs will significantly contribute to achieve nearly grid-independent systems (Calise et al., 2021a).

In the realm of ESS, lithium-ion batteries (LIB) is currently the most reliable and mature technology (Shi et al., 2018), being extensively used in various light electric devices (Fei et al., 2023) (e.g. laptops) and electric vehicles (Fan et al., 2023). However, the extensive use of lithium is straining its supply chain, leading to rising costs for this technology in the coming years (Flexer et al., 2018). Lithium is indeed classified as a

* Corresponding author.
E-mail address: francescoliberato.cappiello@unina.it (F.L. Cappiello).

https://doi.org/10.1016/j.jclepro.2025.145254
Received 13 September 2024; Received in revised form 13 February 2025; Accepted 7 March 2025
Available online 22 March 2025

Nomenclature

COP	coefficient of performance of heat pumps [-]
c_p	specific heat capacity at constant pressure [kJ kg^{-1} K^{-1}]
C_{inv}	capital cost [€]
c_v	specific heat capacity at constant volume [kJ kg^{-1} K^{-1}]
E	energy [kWh]
J	specific cost (purchasing) or price [€]
LHV	Lower Heating Value [kWh Sm^{-3}]
$\dot{m}$	*mass flow rate [kg* s^{-1}*]*
NPV	Net Present Value [€]
P	*power [kW]*
PE	primary energy [kWh/year]
PES	*primary energy saving* [-]
PI	*profitability index* [-]
SPB	simple pay-back period [years]
T	temperature [°C]
U	internal energy [kJ] or [kWh]
UA	overall heat transfer coefficient [W/K]
Vol	volume [m^3]

Greek Symbols

β	compression/expansion ratio [-]
ε	referred to isentropic factor
Δ	*difference* [-]
η	isentropic efficiency/efficiency [-]
ρ	density [kg m^{-3}]
Ψ	pressure level of the tank [%]

Subscripts

a, A	referred to air
air	referred to air
AA-CAES	advanced adiabatic compressed air energy storage system
aux	auxiliary system
available	referred to available excess of renewable electricity
C	compressor
CAES	compressed air energy storage system
CH	chiller
CW	cooling water
deficit	referred to deficit, i.e. demand, of electricity
ETC	evacuated solar collectors
fromCAES	referred to electricity withdrawn from the CAES
fromGRID	referred to electricity withdrawn from the grid
HE	heat exchanger
HEs	referred to heat exchangers
HT	referred to high temperature oil
inlet	referred to the inlet side
INV	inverter
MT	referred to medium temperature oil
N	speed number
outlet	referred to the outlet side
plant	referred to the whole CAES plant
PS	proposed system
PV	photovoltaic field
ref	referred to reference value
rejected	referred to rejected thermal energy
RS	reference system
Rrenew	ratio of renewable energy balancing the overall load of the district
T	turbine
TK	tank
TK-A	referred to compressed air tank
TK-OIL-HT	referred to high temperature oil tank
TK-OIL-MT	referred to medium temperature oil tank
toCAES	referred to electricity exported to the CAES
toGRID	referred to electricity exported to the grid
W	referred to water
Useful	referred to useful thermal energy
USER	referred to the thermal energy demand of the district

critical raw material by a European study on Critical Raw Materials for Strategic Technologies and Sectors in the European Union (Maisel et al., 2023). Moreover, the majority of LIB components (roughly 86 %) are supplied by Asian companies, determining severe issues in terms of market availability and competition (Bibra et al., 2022). Another critical issue regards the rare earth materials which are crucial for producing lithium battery (Abe et al., 2024). In this regard, the ongoing trade dispute between the U.S. and China over rare earth materials underscores the strategic importance of these elements. The U.S. is taking steps to reduce its dependency on Chinese imports through importing duties and investments in domestic production, while China is tightening its control over rare earth processing technologies. These developments are likely to have far-reaching implications for global supply chains, technology manufacturing, and national security strategies (Politico. U, 2024). This would make the price of the lithium-battery to fluctuate under the international crisis (Zhang et al., 2024a). LIBs are not considered suitable for high-capacity ESS, specially for balancing unpredictable renewable energy sources like solar and/or wind (Calise et al., 2023b). Hydrogen-related technologies are considered one of the best alternatives for high capacity electric energy storage (Hernandez and Gençer, 2021). The European Union is trying to push the research and industrialization of hydrogen related technologies (E. Comission). However, this goal is far to be achieved, indeed these technologies are featured by extremely high capital costs (Böhm et al., 2020), and studies on renewables integrated with hydrogen as alternative ESS often show poor economic profitability (Calise et al., 2022).

In this framework, compressed air energy storage (CAES) can compete with hydrogen and lithium-ion battery, in terms of performance, capital costs (Tong et al., 2021), scalability, durability and sustainability (Bazdar et al., 2022). CAES main drawbacks are: low roundtrip efficiency (RTE), high response time, and low depth of discharge (Bazdar et al., 2022). Despite these limitations, combining CAES with renewable power generation is considered one of the most promising solutions for addressing the intermittency of renewable energy (Assareh and Ghafouri, 2023). The operating principle of CAES is similar to the one of pumped-hydro power plants (Ardizzon et al., 2014), using air instead of water as energy carrier. Ambient air is compressed and stored in suitable storage systems such as tanks (Zhang et al., 2023), underground caverns (Han et al., 2022), or geological porous formation (Gasanzade et al., 2023). When electric demand exceeds renewable production, the pressurized air is heated and expanded in a turbine to generate electricity. A crucial aspect of CAES involves the design of a proper cooling system since compressing air from atmospheric pressure to storage pressure in a single stage is extremely energy intensive, whereas using multi-stage compression with intercooling stages significantly enhances system efficiency (Salvini and Giovannelli, 2022; Liu et al., 2023; Moran et al. 2014). Simultaneously, the power produced by a gas expansion may be significantly enhanced by increasing the temperature of the inlet fluid (Moran et al. 2014). Therefore, conventional CAES systems employ fossil fuels to increase gas turbine inlet temperatures, increasing the system power production (Baqari and Vahidi, 2013). Furthermore, turbines represent a bottle neck for CAES systems, limiting the RTE of CAES to 40 %–55 % due to the need for external heat to increase their inlet temperatures (Budt et al., 2016).

Adiabatic CAES (A-CAES) technology aims to overcome the drawbacks of conventional CAES systems (Courtois et al., 2021), using the compression heat to reheat turbine inlet air, by using a suitable thermal storage (Razmi et al., 2021a). This approach can potentially improve the RTE up to 50–70 %, but a complex thermal management must be developed (Zhang et al., 2024b), also including the minimization of thermal losses (Zhang et al., 2024b).

The open literature includes several studies dealing with different aspects of CAES. Dib et al. (2021) presented a thermodynamic and energy analysis of two types (mechanical piston vs liquid-piston) of isothermal compression technologies, including detailed mathematical models. The models showed that mechanical piston technology is favorable for producing hot water during compression and cold water during expansion, while liquid piston technology shows a quasi-isothermal performance. However, attaining near-isothermal compression and expansion is extremely challenging due to the rapid and energy-intensive heat transfer required. Innovative solutions, such as spray cooling, are being investigated at the theoretical stage and have shown potential RTE values greater than 75 % (Chen et al., 2020a). However, this kind of technology is at the precommercial stage and is mainly designed for small applications. Furthermore, achieving isothermal conditions is technically challenging and requires advanced engineering solutions which are complex and expensive.

To address the main limitation of A-CAES, advanced adiabatic compressed air energy storage (AA-CAES) systems (Budt et al., 2016) are increasingly being explored. AA-CAES integrates the principles of A-CAES with renewable energy sources. In this configuration, renewable energy sources are used to further increase the turbine inlet temperature, increasing the overall system efficiency (Zhao et al., 2021). In ideal conditions (no thermal drops and pressure drops, ideal gas, etc), AA-CAES can achieve RTE up to 75 %, whereas real RTE values are around 60 %, highlighting the gap between theoretical and practical efficiencies (King et al., 2021).

Several studies in the scientific literature investigate hybrid systems that integrate renewable energy sources with CAES technology (Ghalelou et al., 2016), considering: wind (Razmi et al., 2021b), solar (Alirahmi et al., 2021), and biomass gasification (Diyoke and Wu, 2020). Many of these studies focus on improving system efficiency by integrating CAES with smart grids (Venkataramani et al., 2016), polygeneration plants (Jiang et al., 2021) for heating, cooling, and power, cogeneration plants (Vieira et al., 2021), or energy cascade utilization involving ORC (Du et al., 2022) or Kalina cycles (Piri et al., 2023) as bottoming cycles. Recently, Hai et al. (2023) investigated a polygeneration system that combines a biomass gasifier-fired steam Rankine cycle with a CAES system. In this configuration, the power generated by the Rankine cycle is used to supply the electric heater and compressor of the CAES system. Additionally, an absorption chiller and a heat exchanger are included to produce, respectively, domestic hot water and cooling energy using the waste heat from the gasifier-fired steam Rankine cycle. A fraction of the power is also supplied to a proton exchange membrane (PEM) electrolyzer to produce hydrogen. Energy, exergy, exergoeconomic and environmental analyses were performed, achieving an exergy RTE of 41.21 %, a total cost rate of 708.14 $/h, and a unit cost of multi-generation of 0.072 $/kWh. The work is based on the steady-state assumption. Therefore, the turbomachines (compressor and turbine) are modelled using a simple constant isentropic efficiency model, which may lead to relevant errors, considering that compressors and turbines operate under off-design conditions (partial load) (Rahbari and Arabkoohsar, 2021). During the charging phase, the CAES system must track the available surplus power delivered to the compressors and the pressure inside the tank. Conversely, during the discharging phase, the system must follow the required power and the pressure inside the tank. Under these operating conditions, the RTE is lower than that achieved at rated load, i.e. under steady-state conditions (Chen et al., 2020b). The energy and exergy efficiency of a CAES system at rated load can reach up to 65 %, whereas at partial load operation (30 %), both efficiencies drop below 45 %.

Optimal control strategies are pivotal for an efficient management of CAES systems under off-design conditions. Zhang et al. (2021) proposed the integration of an inverter-driven compressor between the compressed air tank and the turbine train, to control the turbine inlet pressure. Thus, the turbine operates at constant inlet pressure, but an additional compression work is required to this scope. This measure reduces the losses associated with the throttling valve, improving the system RTE by 1.8 %–2.7 %, also achieving constant isentropic efficiency for turbines and compressors because the inverter-driven compressor decouples their operation from the tank pressure level.

Yao et al. (2023) investigated a novel trigenerative system that integrates compressed air and chemical energy storage. In this system, the heat generated during compression is used to decompose methanol and produce high-temperature syngas which can be stored and used as a fuel to drive the operation of a gas turbine. The residual heat from the system is also used to simultaneously produce cooling and heating energy via an ammonia-water absorption chiller. A multi-objective optimization was conducted to determine the optimal operating parameters of the air compressor and gas turbine from thermodynamic, economic, and environmental perspectives. The entire plant is simulated under steady-state conditions. The best solution achieved an exergy RTE of 42.96 %, a levelized cost of energy (LCOE) of 105.28 $/MWh, and CO_2 emissions of 206.94 kg/MWh of energy output.

Jannelli et al. (2014) explored a novel polygeneration small-scale CAES system for a stand-alone renewable energy power plant based on PV solar panels. The 33 kW PV field is designed to meet the energy demand of a radio base station for mobile telecommunications. This work introduces two main innovations: i) the use of a small-scale CAES system coupled with a thermal energy storage unit with inter-heating expansion and inter-cooling compression; ii) the production of cooling energy using the cold air available at 3 °C from the outlet of the last turbine in the CAES. The proposed system achieved an efficiency of 57 %. However, the results of the study are limited by the constant polytropic efficiency approach used for modeling the compressors and turbines.

Guo et al. (2019) proposed a 10 MW A-CAES plant integrated with a waste heat recovery system. The performance of the compressors and turbines are modelled using the Wide Range of Conditions Model (WRCM), which is widely known for off-design simulations of turbomachines (Ma et al., 2023) and was first developed in (Zhang and Cai, 2002). Despite innovative, WRCM lacks effectiveness in mimicking the real operation of the compressors, as it only provides relationships between dimensionless parameters, useful for theoretical analysis but not practical for real-world compressor simulation. The system proposed by Guo et al. (2019) is designed to follow fluctuating power demand and surplus. However, a major limitation of this research is the installation of a throttling valve between the air tank and the turbines, resulting in a constant pressure air flow rate being delivered to the turbines regardless of the power demand. This type of regulation is highly dissipative and reduces the overall energy performance of the plant. Despite this, simulations indicate that the proposed system achieves a RTE of roughly 70 % under steady-state conditions.

1.1. Aim and novelty of the work

The presented literature review proves the growing interest in CAES as a promising electric energy storage technology. The analysis of the off-design performance of CAES plant is a crucial point. In fact, when the CAES is used as an ESS, the compressors track the available surplus power and the pressure inside the tank, whereas the turbines track the power demand of the user and the pressure inside the tank. Therefore, a steady state analysis can be useful in design phase, but it can lead to nonrealistic results (errors in isentropic efficiency calculations and operating points falling outside turbomachineries operating maps) if used for simulating the transient performance of the whole CAES plant

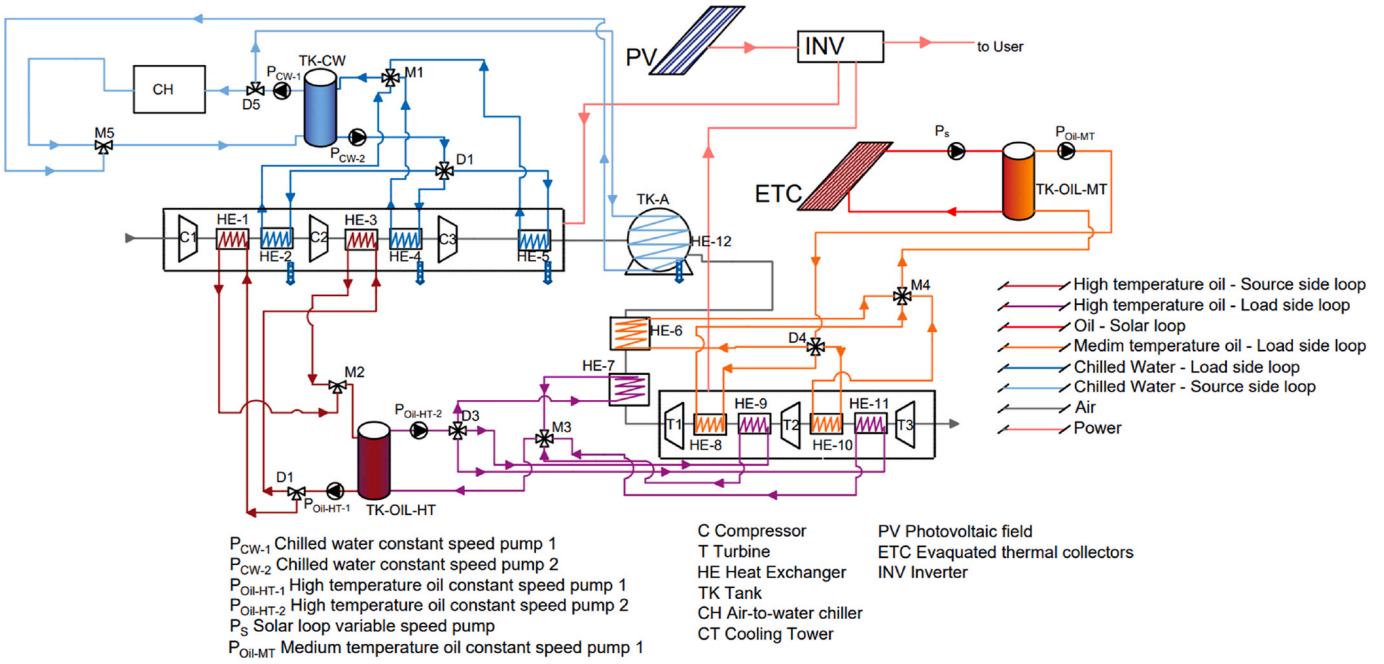

Fig. 1. Proposed CAES layout.

(Logan, 2003). WRCM was developed to this scope (Zhang and Cai, 2002), providing analytical relationship for the main operating parameters of compressor and turbine, i.e. reduced mass, compression ratio, isentropic efficiency, and reduced speed. Given the design conditions of the selected turbomachine, its performance can be simulated by means of the analytical correlation functions. A significant number of research works rely on this approach for modelling the off-design operation of compressors and turbines (Guo et al., 2019).

To the best of the authors' knowledge, two mains limitations are included in the WRCM model. The first one concerns the validation of this model, which is quite questionable since it is based only on an old reference, only available in Chinese language (Zhang et al., 1996). The second limitation regards the fact that WRCM approach does not take into account the performance map of the turbomachines. Therefore, the WRCM curves are only theoretical operating points, as suggested by Refs. (Zhang and Cai, 2002). and (Guo et al., 2019), potentially including unfeasible operating points, falling outside the turbomachineries operating maps (Logan, 2003).

In this framework, this paper proposes a novel approach for assessing the off-design performance of a CAES plant operating under variable dynamic conditions, based on a co-simulation approach. This proposed approach integrates a dynamic model, developed in TRNSYS of the whole plant. While the performance of the included turbomachine is assessed by means of the performance maps of turbines and compressors provided by the manufacturer. In particular, such performance maps are developed in the steady state condition. For this reason, the provided dynamic model relies on the quasi-steady state assumption, where the features and properties of the whole plant are dynamically assessed, whereas the features and the properties of the turbomachines are assumed in quasi-steady state conditions by means of the performance maps. This algorithm is used for accurately simulating the time dependent performance of an AA-CAES technology, used as electric energy storage system, storing the surplus PV power production, and matching the electricity demand of a fully electric residential district. Each stage of compression is intercooled, while each turbine stage is preheated, exploiting the waste heat due to compressors work and due to an evacuated solar thermal collectors field.

For the sake of clarity, the main novelties of this paper are here highlighted:

- A detailed model of compressors and turbines based on performance maps provided by the manufacturer. Therefore, the proposed model can mimic the real off-design operation of turbines and compressors discarding all the operating points out of the performance maps.
- A detailed model of the air compressed tank taking into account the internal energy variation due to filling/emptying process.
- A dynamic co-simulation model of an AA-CAES serving a fully electric residential district as electric energy storage system, storing the excess photovoltaic electricity.
- A detailed dynamic model of the thermodynamic performances of the whole plant, also considering the heat transfer rates occurring within the plant. This point is a key aspect in the analysis. In fact, the thermal energy recovered from the compression work and supplied to the compressed air delivered to the turbine significantly affects the performance of the whole plant. In this framework, the heat exchange occurring in each stage is carefully modelled and dynamically addressed.

2. System layout

Fig. 1 shows the layout of the proposed AA-CAES plant, designed to shave the peaks of power demand in a residential district. The power demand of the district is met by a photovoltaic (PV) field. When PV power production exceeds the power demand of the residential district, the surplus electricity is used to drive the compression train, which compresses the outdoor air. Specifically, the compression train is activated only when the power surplus exceeds the minimum activation power of the compressors, a value that varies depending on the tank pressure. This plant includes a train of three compressors: compressors C1 and C2 are centrifugal compressors, while C3 is a reciprocating compressor. The compression phase is split in three intercooled compressions in order to reduce the overall compression work. This arrangement is selected according to manufacturer reports, suggesting that for high pressure fluids alternative compressors should be preferred to centrifugal compressors (Burckhardt Compression; Air Liquide; BellissMorcom; Reavell; Copco, 2024). The suction air entering the first compressor, C1, is compressed as a consequence C1 outlet temperature is also very high. To reduce the overall compression work, two intercooling heat exchangers in series, HE-1 and HE-2, are used to reduce C2

inlet temperature. HE-1 and HE-2 operate using diathermic oil and water as cooling fluid, respectively, recovering a significant amount of waste heat.

The cooled air is then supplied to C2, where undergoes compression. The air at the delivery of C2 is further cooled by two heat exchangers, HE-3 and HE-4. HE-3 uses diathermic oil as cooling fluid. HE-4 operates using water as cooling fluid. The air stream at the outlet of HE-4 is supplied to the third compressor, C3, which is a reciprocating compressor with a constant pressure ratio (β) of 2.0. Finally, the air is cooled by HE-5, which operates with water as cooling fluid. This cooling step is crucial to reduce the temperature of the air delivered to the compressed air tank (TK-A). In fact, during the tank charging phase, a remarkable increase of the temperature of the tank is achieved. The rate of this temperature increase depends on the temperature and mass flow rate of the air fed to the tank. This is explained in detail in the section *System Model*. Cooling the air before it enters the tank limits the tank heating and increases the mass of air stored. Lowering the air temperature reduces its pressure increase, allowing more air to be stored before reaching the tank maximum allowable pressure.

The cooling process of the compression train is based on two types of heat exchangers: oil-driven and water-driven. The oil-driven heat exchangers (HE-1 and HE-3) are designed to maximize waste heat recovery from compression. When the compressors are operating, the constant speed pump P-oil-HT-1 is activated, delivering oil to both HE-1 and HE-3 with the same oil mass flow rate. The heated return oil is stored in the stratified oil tank T-OIL-HT. The thermal energy stored in this tank is used for heating the air entering the turbines during the expansion process, producing electricity. The water-driven heat exchangers (HE-2, HE-4 and HE-5) are designed to reduce the air temperature close to ambient temperature. When the compressors are operating, the constant speed pump PCW-2 is activated, supplying cooling water to these heat exchangers at a consistent flow rate. The water loop is balanced using an electric air-to-water chiller (CH). When the bottom temperature of the tank TK-CW ($T_{TK\text{-}CW,bottom}$) exceeds the upper limit of 30 °C, the pump PCW-1 is activated, delivering water to the air-to-water chiller (CH) until $T_{TK\text{-}CW,bottom}$ is cooled below the threshold value of 20 °C.

An evacuated tubes solar thermal collector field (ETC) is integrated into the plant to preheat the air stream supplied to the turbines. The diathermic oil is heated by the ETC field and stored in the TK-OIL-MT tank. This thermal energy is then used for preheating the air supplied to the turbines. Note that the solar loop is managed by a variable speed pump P_S driven by a feedback controller, steering the oil temperature at the outlet of the ETC at 200 °C.

When the PV power is insufficient to meet the residential district power demand, the compressed air is withdrawn from the compressed air tank and supplied to the turbines. This plant includes a train of three radial turbines. The expansion phase is divided in three inter heated expansions in order to increase the overall produced work. First, the air withdrawn from the tank is preheated by heat exchangers HE-6 and HE-7. HE-6 operates with medium-temperature diathermic oil provided by TK-OIL-MT, which is heated by the ETC. The air exiting HE-6 is further heated by HE-7, which uses high-temperature oil (TK-OIL-HT), heated by waste heat recovered from compression. HE-7 heats the air up to 280 °C. In particular HE-7 is managed by a feedback controller selecting the proper mass flow rate of oil to deliver to this heat exchanger in order to get an outlet air temperature of 280 °C. This preheated air is then delivered to the first turbine, T1, where the air inlet enthalpy flow is partially converted into mechanical work, i.e. electricity. After the expansion occurring in T1, the air stream is then heated by HE-8, using medium-temperature oil, and HE-9, using high-temperature oil. The reheated air is supplied to the second turbine, T2. Again, after the expansion the air stream is further heated by HE-10, using oil from the solar tank, and HE-11, using oil from TK-OIL-HT, before entering the last turbine, T3, where it expands to ambient pressure.

During the discharging phase, the temperature of the compressed air tank (TK-A) decreases due to the reduction of internal energy as the tank empties, see *System Model* section. Managing the tank temperature is pivotal to avoid a decrease in the system roundtrip efficiency (RTE). A decrease of the tank temperature also determines a decrease of its pressure, resulting in a lower air mass flow rate. To address this issue, a heat exchanger (HE-12) is installed on the TK-A. When the temperature of the compressed air tank (TK-A) is higher than 20 °C, the pump *PCW-1* is not activated. When the temperature drops to 20 °C, PCW-1 is activated, supplying water to HE-12. This pump supplies both the chiller (CH) and HE-12. If the temperature of TK-CW exceeds 30 °C, the pump is activated to cool the water through the chiller. At the same time, if TK-A temperature drops below 20 °C, the pump feeds water to HE-12. The pump is managed by a feedback controller designed to maintain the temperature of TK-A at 20 °C. A suitable amount of water is delivered to HE-12 to keep TK-A at 20 °C. Note that the same water used for cooling the compressors is used to heat TK-A, reducing the need for the chiller and saving electricity, thereby enhancing plant efficiency.

The pre-heating performed in heat exchangers HE-6 to HE-11 is crucial for increasing the enthalpy of the air stream and maximizing the electricity production. Note that heat exchangers HE-6, HE-8, and HE-10 operate with oil heated by the solar loop. When the turbines are in operation, pump $P_{OIL\text{-}MT}$ is activated, withdrawing a constant amount of oil from the tank TK-SOL-OIL and delivering it to these heat exchangers. At the same time, pump $P_{OIL\text{-}HT}$ is activated, supplying oil to heat exchangers HE-7, HE-9, and HE-11. The oil loop is managed by a feedback controller that adjusts the oil flow rate to each heat exchanger to achieve an outlet air stream temperature of 280 °C. Each oil-driven heat exchanger is specifically designed to heat the air to this target temperature, ensuring optimal performance and maximum electricity generation.

3. Simulation model

The overall dynamic model of the whole plant was developed in TRNSYS18 environment. TRNSYS environment is widely used in both academic and commercial fields (Calise et al., 2023a; Klein et al., 2004). This software is well known for its reliability and accuracy in dynamically simulating plants involving renewable energy sources (Calise et al., 2023a; Cappiello and Erhart, 2021; Bordignon et al., 2021; Figaj, 2021; Angrisani et al., 2014). The models for the compressors train, heat exchangers, turbines train, and compressed air tank are not included in TRNSYS library. Therefore the models of such components were suitably developed in MALTAB by the authors by using the state of the art algorithms. A suitable co-simulation approach was used to link MATLAB and TRNSYS simulations, by using Type 155 routine. For sake of brevity, only the descriptions of the in-house developed models are provided. Note that the in-house models are validated by a code-by-code approach, as explained in the following sections. Concerning the co-simulation model developed in TRNSYS, each model of TRNSYS is validated (Klein, 1988), for this reason the whole plant can be considered validated as a whole. This approach is considered reliable and widely adopted in open literature (Bordignon et al., 2021; Figaj, 2021; Angrisani et al., 2014; Klein, 1988; Calise et al., 2024; Ahamed et al., 2020).

3.1. Compressors train model

The operation of the compressors train is constantly in off-design conditions due to the need to track the available power provided by the renewable energy source ($P_{el,available}$) and the pressure inside the tank ($P_{ress,TKa}$), which increases during the charging phase. In addition, the temperatures of the diathermic oil tank and water tank rise due to the waste heat discharged by the air in the intercooling heat exchangers (see Fig. 1). To address these variable conditions, a suitable tool was developed to dynamically assess the real operating point of each compressor and the whole compressors train. This tool can detect the real operating point of each compressor according to the real performance map

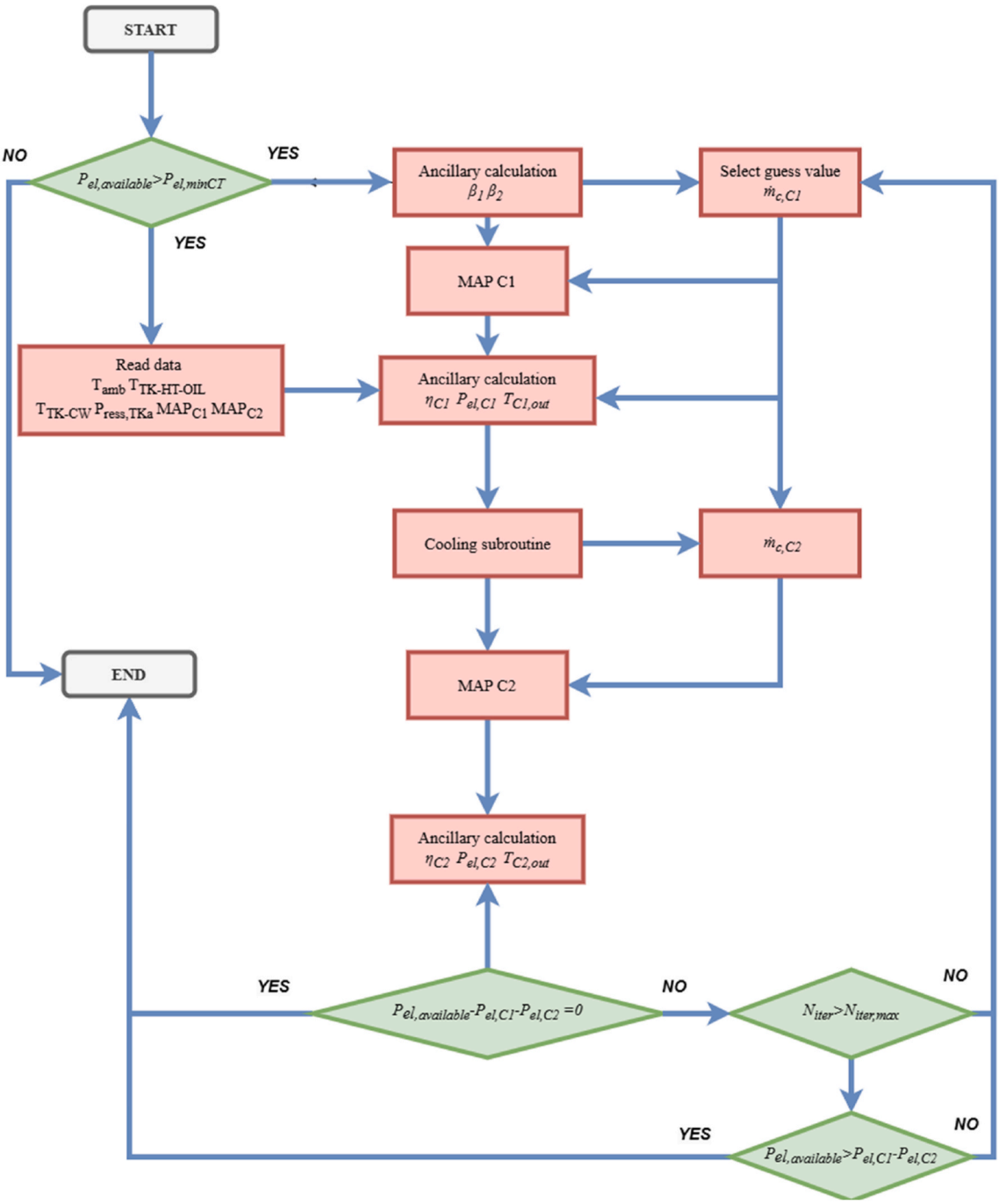

Fig. 2. Flow chart of the algorithm searching the operating point of the compressor train.

provided by the manufacturer. It assesses the corrected mass flow rate ($\dot{m}_{c,C}$), compression ratio (β_C), corrected compressor speed ($n_{c,C}$) and isentropic efficiency (η_C) at each time step. Moreover, it ensures that the operating points fall within the acceptable range defined by the performance map, rejecting any solutions outside this range. Given the available renewable power ($P_{el,available}$), tank pressure ($P_{ress,TKa}$), and the temperatures of the outdoor air, oil and water tanks, this tool dynamically mimics the real operation of each compressor, discarding all non-allowed operating points.

For this work, the compressor map of the ASME 95-GT-79, provided by GSP software (Xu et al., 2021; Calise et al., 2007) and Gasturb database (Calise et al., 2007; Boyce and Rao), is used. Since this map does not match the requirements of the developed plant, it is scaled according to the design capacity of the proposed plant using the similarity approach (Xu et al., 2021; Wang et al., 2017). The similarity method is a reliable and widely adopted method for scaling the map of turbomachinery to the design capacity of a developed system (Xu et al., 2021; Wang et al., 2017).

The developed tool, implemented in the MATLAB environment, assesses the operating point of the compressor train based on the performance map of each compressor. Given the pressure of the air tank ($P_{ress,TKa}$) and the available surplus power ($P_{el,available}$) as input variables, the tool iteratively searches for the operating condition of the entire train, see Fig. 2.

The tool starts by assessing the compression ratio of the whole train and the number of compressors that need to be activated along with their respective compression ratios, see Eq. (1a) and Eq. (1b). Note that the third compressor is a volumetric compressor featured by a constant

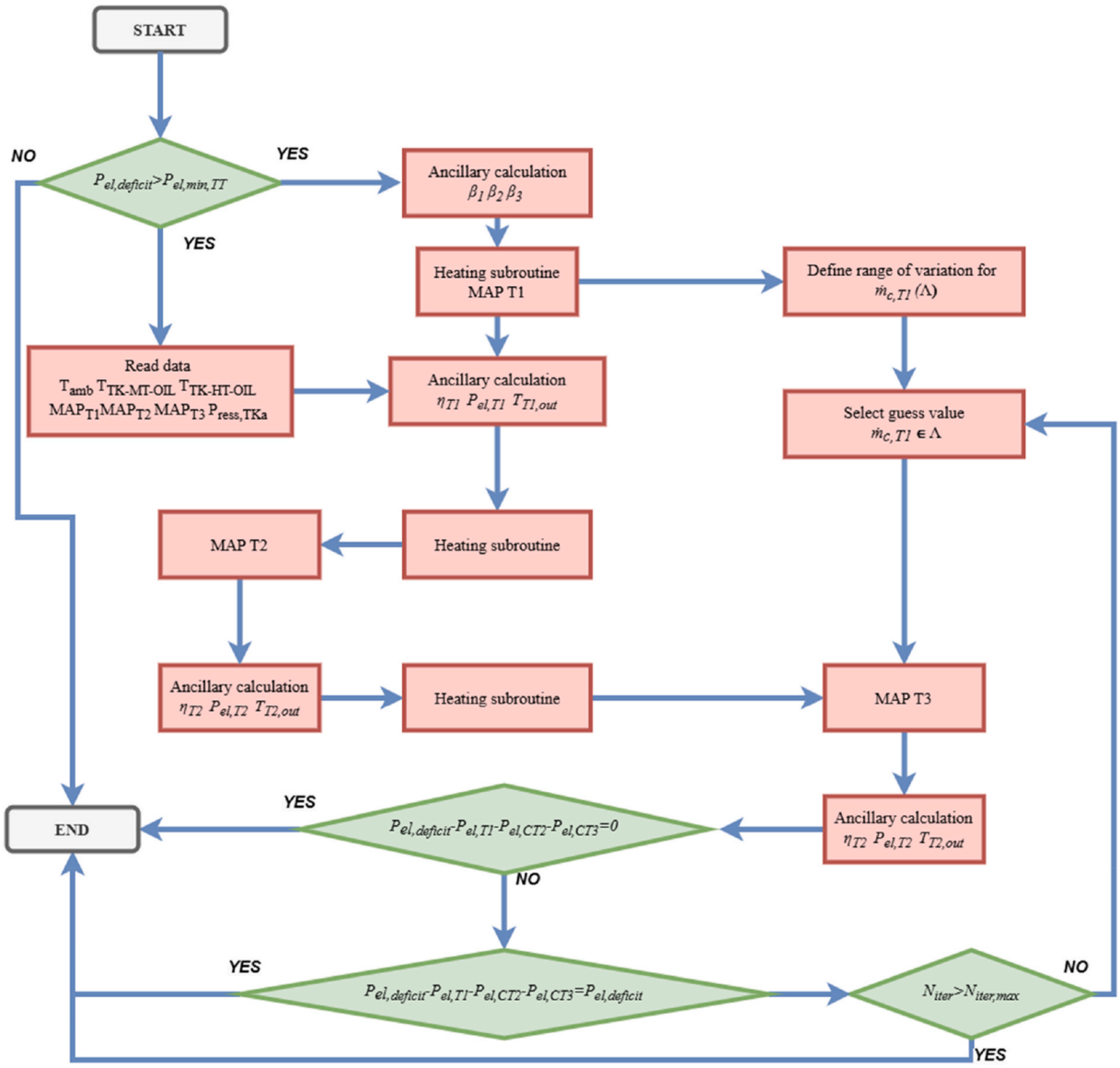

Fig. 3. Flow chart of the algorithm searching the operating point of the turbines train.

compression ratio ($\beta_{C3} = 2.0$).

$$\beta_{plant} = \frac{P_{ress,TKa}}{P_{ress,atm}} \tag{1a}$$

$$\begin{cases} \beta_{C1} = \beta_{C2} = \sqrt{\beta_{plant}} & \beta_{plant} < 350bar \\ \begin{cases} \beta_{C1} = \beta_{C2} = \sqrt{\beta_{plant}/\beta_{C3}} \\ \beta_{C3} = 2.0 \end{cases} & \beta_{plant} \geq 350bar \end{cases} \tag{1b}$$

The air is modelled as an ideal gas. This assumption was mainly performed in order to reduce the computational effort to run the developed model. However, such assumption is validated using a code-to-code approach: the results from this routine are compared against those based on real gas models, returned by Refprop (Lemmon et al., 2007), a reference software widely used for fluid property calculations (Bordignon et al., 2021; Lemmon et al., 2007; Rane et al., 2021; Wang et al., 2024; Sheng et al., 2023; Ding et al., 2024; Bertini et al., 2021). Note that this assumption leads to an error around 4.4 % in assessing the mechanical work of the compressors train. However, this assumption is needed for reducing the computational effort of the proposed model, which must be run thousands of times (depending on the selected time-step) in TRNSYS for a 1-year simulation of the system as a whole. In particular, such approach is 56 % faster with the one adopting the real gas model for the air modelling.

Note that in Eq. (1b) it is assumed that both C1 and C2 operate with the same compression ratio. This assumption is consistent with the results available in the thermodynamic analysis, in case of constant isentropic efficiencies, as shown references (Moran et al. 2014; Volpe, 2011). However, the isentropic efficiency of the compressor changes as the compression ratio changes. Therefore, the optimal value of the pressure ratio of the first compressor should be determined dynamically for each operating point. This operation could be performed by a controller aiming at maximizing the air mass flow rate, for each value of the available excess electricity produced by the renewables. However, this is an extremely complex controller due to the non linearity and non convexity of the domain. Therefore, for sake of simplicity, the present study considers the optimal pressure ratios suggested by a simple thermodynamic analysis. This assumption is supported by the results of several simulations showing that, changing the compression ratio among the compressors, a difference lower than 1 % is detected in the

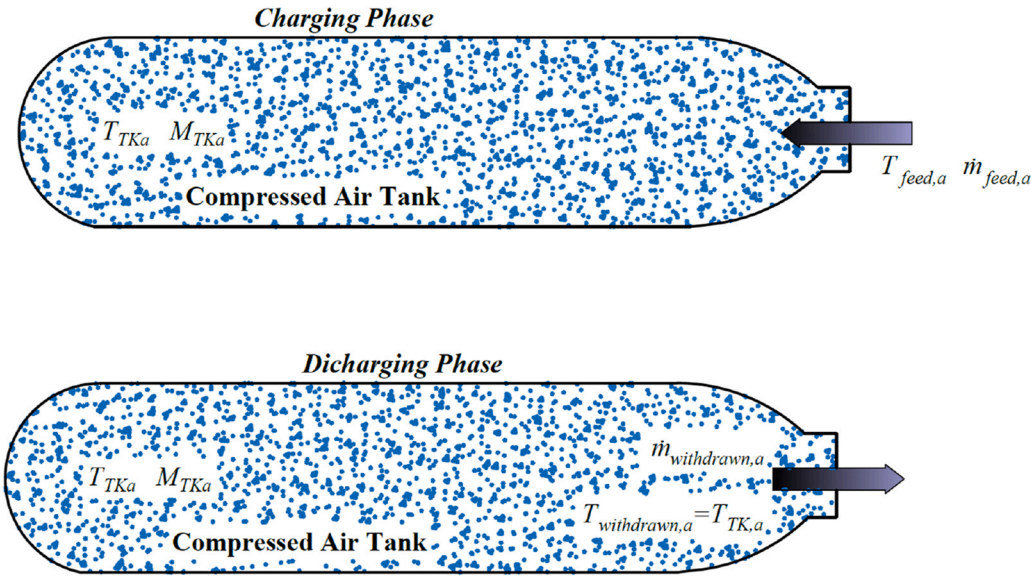

Fig. 4. Tank model: charging phase (above) and discharging phase (below).

Table 1
Design and operating parameters.

Parameter	Description	Value	Unit
$j_{el,fromGRID}$	Electricity purchasing cost	0.30	€/kWh
$j_{el,toGRID}$	Electricity energy exporting cost	0.05	€/kWh
J_{ETC}	ETC specific cost	300 (Calise et al., 2019b, 2020)	€/m^2
J_{PV}	PV specific cost	1000 (Cappiello and Erhart, 2021)	€/kW
J_{oil}	Therminol 66 specific cost	5.65 (Calise et al., 2023a)	€/kg
J_C	Compressor capital cost	$J_C = 5840\ (P_{el,C,rated})^{0.82}$ (Calise et al., 2007; Luyben, 2018)	€
J_T	Turbine capital cost	$J_T = [-98.328 \log(P_T) + 1318.5] P_T$ (Calise et al., 2007; Traverso et al. 2004)	€
J_{pump}	Pump capital cost	$J_{pump} = 1.08(-2.10^{-8} n\&^2 + 0.0285\ n\& + 388.14)$ (Calise et al., 2020)	€
J_{HE}	Heat exchanger capital cost	$J_{HE} = 130.1.4 \left[\left(\frac{A_{HE}}{0.093}\right)^{0.78}\right]$ (Calise et al., 2021b)	€
$J_{TK\text{-}O}$	Oil tank capital cost	$J_{TK} = 494.9 + 0.808\ V_{TK-O}$ (Calise et al., 2014)	€
$J_{TK\text{-}A}$	Compressed air capital tank	$J_{TK-A} = 11394\ V_{TK-A}$ (Calise et al., 2007)	€
J_{CT}	Cooling towers specific cost	36 (Calise et al., 2021b)	€
J_{CH}	Chiller specific cost	150 (Cappiello and Erhart, 2021)	€
η_{el}	Conventional thermo-electric power plant efficiency	46	€/kWh
F_{el}	CO_2 equivalent emission factor for electric energy	0.48	kgCO_2/kWh

Table 2
Envelope features-for each building (Calise et al., 2020).

Building element	Building A & B & C & D			
	U-value [W/m^{2}K]	**Thickness** (m)	ρ_s (−)	ε (−)
Roof	0.916	0.255	0.4	0.9
Façades	1.204	0.240		
Ground floor	1.030	0.285		
Adjacent ceiling	1.157	0.295		
Windows glass	2.89	0.004/0.016/0.004	0.13	0.18

compression work of the compression train.

Then the tool starts with a guess operating condition for the first compressor: i.e. a guess corrected mass flow rate value that falls within the performance map of compressor 1 ($\dot{m}_{c,C1}$), Fig. 2.

The corrected compressor mass flow rate ($\dot{m}_{c,C}$) (Boyce and Rao; Boyce and Boyce, 2012; Sforza and Sforza, 2012) is evaluated according to Eq. (2) (Calise et al., 2007).

$$\dot{m}_c = \dot{m} \frac{\sqrt{T_{inlet}/T_{ref}}}{P_{ress,inlet}/P_{ress,ref}} \tag{2a}$$

$$N_c = \frac{N}{\sqrt{T_{inlet}/T_{ref}}} \tag{2b}$$

Where, T_{inlet} and $P_{ress,\ inlet}$ represent the temperature and the pressure of the air entering the compressor, respectively; while T_{ref} and $P_{ress,ref}$ are the reference temperature and the reference pressure, respectively.

Then, the algorithm enters in the performance map of compressor 1 with the couple of values β_{C1} and $\dot{m}_{c,C1}$. The operating point of C1 is identified, including the isentropic efficiency for that operating condition (η_{C1}). Consequently, the temperature of the air exiting the compressor is evaluated according to the following equation:

$$T_{outlet} = T_{inlet}\left[1 + \frac{\beta^{\varepsilon} - 1}{\eta}\right] \tag{3}$$

A specific routine for assessing the cooling of the air downstream of the compressor is used. Two heat exchangers are considered: a high-temperature heat exchanger fed by diathermic oil and a low-temperature heat exchanger fed by water (see also Fig. 1). The heat exchangers are modelled using the ε-NTU method (Kakaç et al. 2020; Kays and London, 1984).

The main assumption regarding the ε-NTU method relies on the fact that the specific heat capacity of the two exchanging fluids can be

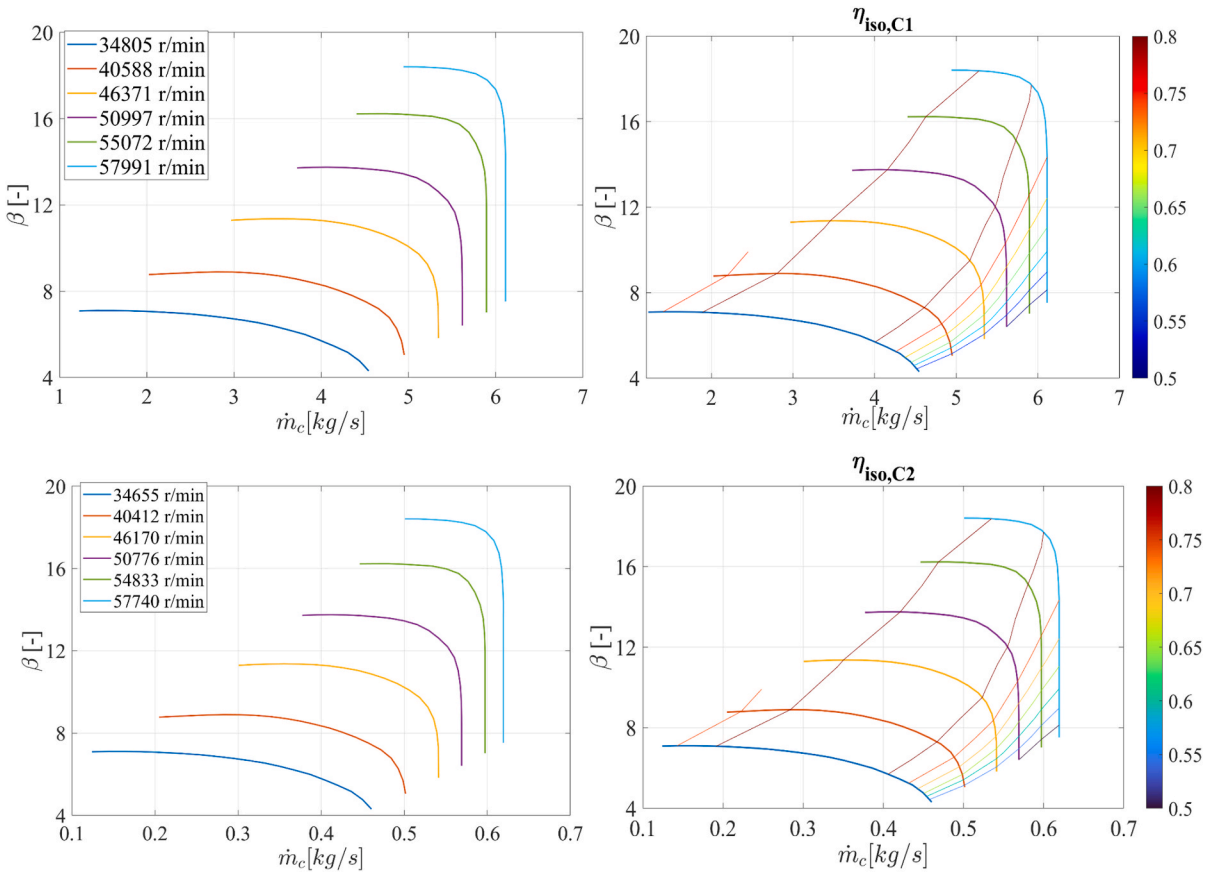

Fig. 5. Compressors maps, obtained from the map of ASME 95-GT-79 (Figaj, 2021; Xu et al., 2021; Calise et al., 2007; Wang et al., 2017): compressor C1 above, compressor C2 below.

considered constant throughout the process and that the enthalpy does not depend on the pressure. However, due to the significant variation in the thermodynamic conditions along the compression train, the specific heat capacity is not considered constant throughout the entire compression train. Therefore, a modified version of ε-NTU method is used, where an average specific heat capacity of each fluid is used. Such parameters are calculated as the ratio between the enthalpy variation and the corresponding temperature variation. This approach is considered reliable and used in several studies (Muscio et al., 2023). Note that the intercooling heat exchangers are assumed to be crossflow heat exchangers. The equation modelling such a heat exchanger is reported below (Eq (4)) (Çengel, 2009).

$$\varepsilon = \frac{1 - exp[-NTUg(1-\overline{\omega})]}{1 - \overline{\omega} exp[-NTUg(1-\overline{\omega})]} \tag{4a}$$

$$\overline{\omega} = \frac{\dot{C}_{\min}}{\dot{C}_{\max}} \tag{4b}$$

This routine returns the temperature of the air exiting the last heat exchanger (HE-2 Fig. 1) and entering the second compressor. Given the mass balance, the mass flow rate entering the second compressor is the same as the mass flow rate entering the first compressor. At this point, the corrected mass flow rate is calculated based on the thermodynamic condition at the inlet of the second compressor according to Eq. (2).

The algorithm then uses the performance map of the second compressor with the values β_{C2} and $\dot{m}_{c,C2}$, assessing the operating point of the second compressor and obtaining the isentropic efficiency for that operating point (η_{C2}).

The algorithm performs a power balance to determine if the identified operating point matches the available power and the given maps of operation for the compressors, as shown in Fig. 2. The following equation is used:

$$P_{el,available}\eta_{shaft} - c_{p,air}\dot{m}_a T_{inlet,C1}\frac{\beta_{C1}^{\varepsilon} - 1}{\eta_{C1}} - c_{p,air}\dot{m}_a T_{inlet,C2}\frac{\beta_{C2}^{\varepsilon} - 1}{\eta_{C2}} = 0 \tag{5a}$$

Where η_{shaft} is the mechanical efficiency of the shaft. It is worth noting that this equation is applicable when only two out of the three compressors are in operation. If the result is zero, the algorithm stops, providing the corrected operating point of the compressor train. If this equation is not satisfied, the algorithm repeats the routine with a new guess corrected mass flow rate value. This means that the algorithm continues to adjust the guess value until Eq. (5a) is satisfied, as shown in Fig. 2. If the algorithm cannot find a solution, i.e. the number of iterations (N_{iter}) exceeds a threshold value ($N_{iter,max}$), a relaxed closing condition is considered, see Eq. (5b) and Fig. 2. This means that if the actual conditions, i.e. available power and tank pressure, lead to an operating point outside the compressors performance maps, the compressors train may use only a share of the available power, Fig. 2. In such cases, the unused power, i.e. $P_{el,unused} = P_{el,available} - P_{el,toCAES}$, is delivered to the grid as excess power.

$$P_{el,available}\eta_{shaft} > c_{p,air}\dot{m}_a T_{inlet,C1}\frac{\beta_{C1}^{\varepsilon} - 1}{\eta_{C1}} + c_{p,air}\dot{m}_a T_{inlet,C2}\frac{\beta_{C2}^{\varepsilon} - 1}{\eta_{C2}} \tag{5b}$$

Note that when all three compressors are in operation the procedure is the same as the one described above, but different equations are considered.

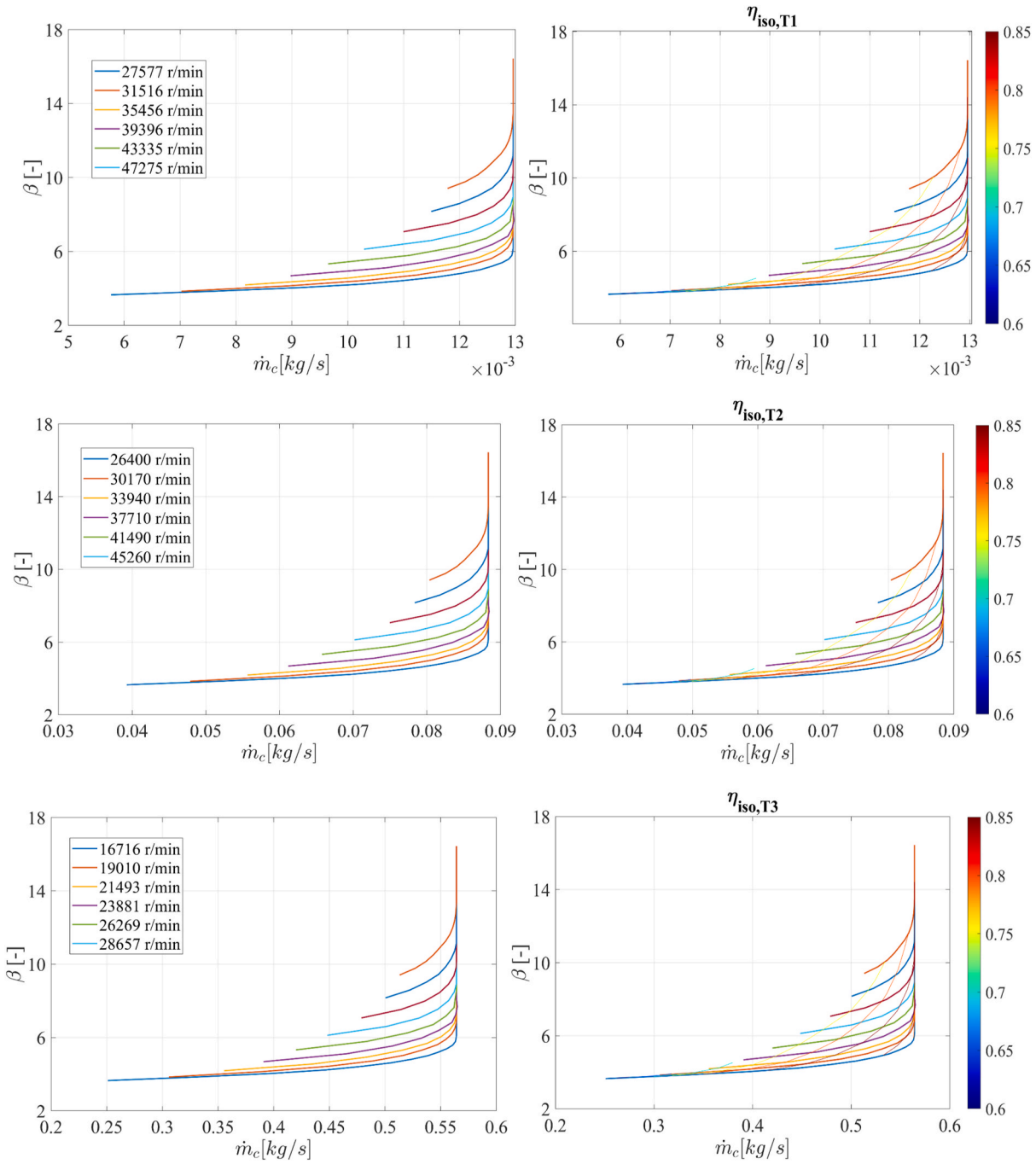

Fig. 6. Turbines maps, obtained from the map of NASA-CR-174646 (Mehigan et al., 2022; Calise et al., 2007, 2019a): a) turbine T1, b) turbine T2 and c) turbine T3.

$$P_{el,available}\eta_{shaft} - c_{p,air}\dot{m}_a T_{inlet,C1}\frac{\beta_{C1}^{\varepsilon}-1}{\eta_{C1}} - c_{p,air}\dot{m}_a T_{inlet,C2}\frac{\beta_{C2}^{\varepsilon}-1}{\eta_{C2}} - c_{p,air}\dot{m}_a T_{inlet,C3}\frac{\beta_{C3}^{\varepsilon}-1}{\eta_{C3}} = 0 \quad (6a)$$

$$P_{el,available}\eta_{shaft} > c_{p,air}\dot{m}_a T_{inlet,C1}\frac{\beta_{C1}^{\varepsilon}-1}{\eta_{C1}} + c_{p,air}\dot{m}_a T_{inlet,C2}\frac{\beta_{C2}^{\varepsilon}-1}{\eta_{C2}} + c_{p,air}\dot{m}_a T_{inlet,C3}\frac{\beta_{C3}^{\varepsilon}-1}{\eta_{C3}} \quad (6b)$$

Here, the second equation (eq. (6b)) refers to the relaxed closing conditions.

Note that if also the relaxed condition is not satisfied, a maximum number of iterations is considered ($N_{iter,max}$). When the routine exceeds such threshold, i.e. $N_{iter,max}$, the routine is stopped, delivering all the available excess power to the grid. This means that the available excess power and the pressure inside the tank lead to an operating point outside the operating maps of the compressors, i.e. an operating condition that must be rejected.

Finally, once the actual operating point of the compressor train is determined, the algorithm calls an explicit solver to assess the temperature of the air and coolant fluids at each state point, as well as all variables related to the operating point of each compressor (see also Fig. 1) and heat exchangers. This step is crucial, as the proposed model carefully addresses the thermal energy performance of the system, with particular attention to the temperature of the water and oil delivered to

Table 3
Design data of the main components of the plant.

Component	Parameter	Description	Value	Unit
C1	$Type$	Type of compressor	Centrifugal	
	β_{max}	Maximum compression ratio of the compressor	15.0	–
	T_{ref}	Reference temperature	273.15	K
	$Press_{ref}$	Reference pressure	1.013	bar
C2	$Type$	Type of compressor	Centrifugal	
	β_{max}	Maximum compression ratio of the compressor	15.0	–
	T_{ref}	Reference temperature	273.15	K
	$Press_{ref}$	Reference pressure	1.013	bar
C3	$Type$	Type of compressor	Alternative	
	β_{max}	Maximum compression ratio of the compressor	2.0	–
	T_{ref}	Reference temperature	273.15	K
	$Press_{ref}$	Reference pressure	1.013	bar
Compression Train	$P_{el,max}$	Maximum power of the compression train	3.80	MW
	$P_{el,min}$	Minimum power of the compression train	1.00	MW
T1	$Type$	Type of turbine	Radial	
	β_{max}	Maximum compression ratio of the compressor	7.0	–
	T_{ref}	Reference temperature	273.15	K
	$Press_{ref}$	Reference pressure	1.013	bar
T2	$Type$	Type of compressor	Radial	
	β_{max}	Maximum compression ratio of the compressor	7.0	–
	T_{ref}	Reference temperature	273.15	K
	$Press_{ref}$	Reference pressure	1.013	bar
T3	$Type$	Type of compressor	Radial	
	β_{max}	Maximum compression ratio of the compressor	7.0	–
	T_{ref}	Reference temperature	273.15	K
	$Press_{ref}$	Reference pressure	1.013	bar
Expansion Train	$P_{el,max}$	Maximum power of the compression train	1.50	MW
	$P_{el,min}$	Minimum power of the compression train	0.70	MW
Tk-A	$Press_{max}$	Tank maximum pressure	350	bar
	V	Tank volume	250	m^3
	UA **(HE12)**	Overall heat transfer coefficient of exchanger of Tk-A	15.00	kW/K
	$\dot{m}_{oil,rated}$ **(HE12)**	Rated diathermic oil flow rate	7	kg/s
HE1	$\dot{m}_{oil,rated}$	Rated diathermic oil flow rate	6	kg/s
	UA	Rated Overall heat transfer coefficient of exchanger	15.02	kW/K
HE2	$\dot{m}_{oil,rated}$	Rated diathermic oil flow rate	8	kg/s
	UA	Rated Overall heat transfer coefficient of exchanger	8.8	kW/K
HE3	$\dot{m}_{oil,rated}$	Rated diathermic oil flow rate	6	kg/s
	UA	Rated Overall heat transfer coefficient of exchanger	12.05	kW/K
HE4	$\dot{m}_{oil,rated}$	Rated diathermic oil flow rate	8	kg/s
	UA	Rated Overall heat transfer coefficient of exchanger	8.8	kW/K
HE5	$\dot{m}_{oil,rated}$	Rated diathermic oil flow rate	8	kg/s
	UA	Rated Overall heat transfer coefficient of exchanger	4	kW/K
HE6	$\dot{m}_{oil,rated}$	Rated diathermic oil flow rate	9	kg/s
	UA	Rated Overall heat transfer coefficient of exchanger	7.7	kW/K
HE7	$\dot{m}_{oil,rated}$	Rated diathermic oil flow rate	2	kg/s
	UA	Rated Overall heat transfer coefficient of exchanger	7	kW/K
HE8	$\dot{m}_{oil,rated}$	Rated diathermic oil flow rate	5	kg/s
	UA	Rated Overall heat transfer coefficient of exchanger	7.7	kW/K
HE9	$\dot{m}_{oil,rated}$	Rated diathermic oil flow rate	2	kg/s
	UA	Rated Overall heat transfer coefficient of exchanger	7	kW/K
HE10	$\dot{m}_{oil,rated}$	Rated diathermic oil flow rate	5	kg/s
	UA	Rated Overall heat transfer coefficient of exchanger	7.7	kW/K
HE11	$\dot{m}_{oil,rated}$	Rated diathermic oil flow rate	2	kg/s
	UA	Rated Overall heat transfer coefficient of exchanger	7	kW/K
CH	$Q_{cool,\ rated}$	Rated Cooling Capacity	0.80	MW
	COP	Rated COP	4.0	–
	$\dot{m}_{CH}$	Rated chilled water flow rate	16	kg/s
PV	$P_{el,rated}$	PV rated capacity for proposed system	6.40	MW
	η_{PV}	Rated PV field efficiency	18	%
ETC	A_{ETC}	Evacuated tubes collector area	2000	m^2
	Q_{ETC}	Rated ETC capacity	1.30	MW
	η_{ETC}	Rated ETC efficiency	60	%
	$Tset$	Setpoint of the solar pump	200	°C
Therminol 66	$Tsat\ (Press = 1.01\ bar)$	Stauration temperature at 1.01 bar	359	°C
	ρ	Density	885	kg/m^3
	cp	Specific heat capacity	2.195	kJ/kg K
	ν	Kinematic viscosity	0.9700	mm^2/s

the heat exchangers. This ensures that the thermal energy performance of the plant is accurately modelled.

Compressors C1 and C2 are modelled using the performance map of the ASME 95-GT-79 compressor, provided by GSP software (Calise et al., 2007, 2019a) and the Gasturb database (Mehigan et al., 2022; Calise et al., 2007). This map has been properly scaled using the similarity method as explained above. Compressor C3 is a volumetric reciprocating compressor, specifically a cylinder gas piston compressor (Giampaolo, 2020). The selected compressor operates with a constant compression ratio β_{C3} equal to 2.0, partializing only the mass flow rate processed by the compressor. Given this assumption, the isentropic efficiency of this compressor is considered constant. In fact, each cycle is thermodynamically identical; varying the mass flow rate delivered to this type of compressor only changes the number of cycles (Mauro, 2023).

3.2. Turbines train model

Similar to the compressor train, the turbine train constantly operates under off-design conditions, as it needs to track the residual power demand of the plant/users ($P_{el,deficit}$). Additionally, the pressure and temperature of the air tank decrease during the CAES discharging mode, and the temperature of the oil feeding the heat exchangers also decreases.

Table 4
Yearly results.

Parameter	Value	Unit
$E_{el,LOAD}$	10.65	GWh/year
$E_{el,LOAD(District)}$	10.35	GWh/year
$E_{el,PV}$	10.80	GWh/year
$E_{el,fromGRID}$	4.36	GWh/year
$E_{el,toGRID}$	2.96	GWh/year
$E_{el,fromCAES}$	1.48	GWh/year
$E_{el,toCAES}$	2.48	GWh/year
$E_{el,self}$	6.30	GWh/year
$E_{el,aux}$	0.30	GWh/year
$E_{el,CH}$	0.30	GWh/year
$E_{el,P2C}$	0.30	GWh/year
$E_{th,O\text{-}HT,fromCs}$	1.02	GWh/year
$E_{th,O\text{-}HT,toTs}$	1.01	GWh/year
$E_{th,W,fromCs}$	1.10	GWh/year
$E_{th,W,rejected}$	1.10	GWh/year
$E_{th,O\text{-}MT,fromETC}$	0.88	GWh/year
$E_{th,O\text{-}MT,toTs}$	0.87	GWh/year
$E_{th,Cs}$	2.12	GWh/year
$E_{th,Ts}$	1.89	GWh/year
$E_{th,TK\text{-}a}$	0.04	GWh/year
$E_{el,self}/E_{el,LOAD}$	59.11	%
$E_{el,fromGRID}/E_{el,LOAD}$	40.89	%
$E_{el,fromCAES}/E_{el,LOAD}$	13.93	%
$E_{el,fromCAES}/E_{el,self}$	23.56	%
$E_{el,self}/E_{el,PV}$	58.32	%
$E_{el,toCAES}/E_{el,PV}$	23.00	%
$E_{el,toGRID}/E_{el,PV}$	27.42	%
$\eta_{roundrip}$	59.74	%
$\eta_{roundrip,overall}$	42.40	%
$E_{el,P2C}/E_{el,CH}$	98.74	%
$E_{th,Useful}/E_{th,Cs}$	49.88	%
$E_{th,O\text{-}MT,toTs}/E_{th,Ts}$	46.28	%
$E_{th,O\text{-}HT,toTs}/E_{th,Ts}$	53.72	%
COP	3.49	–
PE_{RS}	22.50	GWh/year
PE_{PS}	3.04	GWh/year
ΔPE	19.47	GWh/year
PES	86.51	%
R_{renew}	59.11	%
C_{RS}	3.20	M€/year
C_{PS}	1.52	M€/year
I	35.71	M€
I_{C+T}/I	65.59	%
ΔC	1.68	M€/year
ΔC	52.57	%
SPB	21.25	years
NPV	−12.04	M€
PI	−0.34	–

Therefore, a suitable simulation model of the turbines train has been developed in MATLAB. This tool can identify the real operating point of the turbines train, discarding any points that fall outside the performance map of the turbines.

In this work, the performance map of the radial turbine NASA-CR-174646, available in the databases of GSP software and Gasturb (Mehigan et al., 2022; Calise et al., 2007, 2019a), is used. Similar to the compressor map, the turbine map is properly scalded according to the plant capacity using the similarity approach (Xu et al., 2021; Wang et al., 2017).

To assess the operating point of the turbines train an iterative algorithm has been developed. Given the required power demand ($P_{el,deficit}$) and the pressure inside the tank ($P_{ress,TKa}$), the expansion ratio of each turbine is evaluated (Fig. 3 and Eq. (7)).

$$\beta_{plant} = \frac{P_{ress,TKa}}{P_{ress,atm}} \tag{7a}$$

$$\beta_{T1} = \beta_{T2} = \beta_{T3} = \sqrt[3]{\beta_{plant}} \tag{7b}$$

The same expansion ratio assumed for both turbines, on the basis of the same discussion reported above for the compressors (Moran et al. 2014). The algorithm uses the map of the first turbine (T1) with the expansion ratio of the first turbine (β_{T1}), assessing all the possible corrected mass flow rates ($\dot{m}_{c,T1}$) that fall within the performance map of T1 and are characterized by this expansion ratio (Λ). The algorithm selects a guessed corrected mass flow rate ($\dot{m}_{c,T1}$) from this set of values ($\dot{m}_{c,T1} \in \Lambda$, Fig. 3). Given this guessed corrected mass flow rate, another problem must be solved to detect the real mass flow rate. Two heat exchangers preheat the air entering the first turbine (T1 see Fig. 1). The corrected mass flow rate ($\dot{m}_{c,T1}$) corresponds to different real mass flow rate values depending on the temperature of the air leaving the heat exchanger HE-7 (Fig. 1), see also Eq. (2). However, heat exchanger HE-7 is managed by a feedback controller designed to select the appropriate mass flow rate of diathermic oil delivered to this heat exchanger to achieve an air outlet temperature of 280 °C. Consequently, the temperature of the turbine T1 inlet air is constantly maintained at the design value of 280 °C. Therefore, the real mass flow rate is evaluated according to Eq. (2).

Given the actual air mass flow rate, the corrected mass flow rate, and the temperature of the air entering turbine T1, the operating point of the first turbine is identified, obtaining the isentropic efficiency (η_{T1}). Then, the power provided by the turbine and the temperature of the air leaving the turbine are evaluated. Specifically, the temperature of the air leaving the turbine after expansion is evaluated using the following equation:

$$T_{outlet} = T_{inlet}\left[1 - \frac{(\beta^{\varepsilon} - 1)}{\eta}\right] \tag{8}$$

The air is modelled as an ideal gas. As explained in the previous section such assumption is validated using a code by code approach. At this point, the preheating subroutine is called. This subroutine models the heat exchange occurring in the heat exchangers HE-8 and HE-9 using the ε-NTU method (Kakaç et al. 2020; Kays and London, 1984). As mentioned in the previous paragraph, the mean specific heat capacity of each fluid is used, such value is assessed according to the thermodynamic conditions between the inlet and outlet of each heat exchanger. This approach is considered reliable and used in several studies (Muscio et al., 2023). In this phase, the subroutine is designed to assess the temperature of the air feeding the second turbine. Given the temperature of the air feeding the second turbine and the actual real mass flow rate, the corrected mass flow rate ($\dot{m}_{c,T2}$) is evaluated according to Eq. (2). Given the corrected mass flow rate ($\dot{m}_{c,T2}$) and the actual expansion ratio (β_{T2}) for turbine T2, the operating point of turbine T2 is identified. The algorithm then enters the performance map of T2 to obtain the isentropic efficiency, assessing the temperature of the air leaving the turbine and the power provided by the turbine. The algorithm then calls the preheating subroutine again for subsequent turbines. Conceptually, the algorithm follows the same step above described, see Fig. 3.

Finally, the algorithm performs the following energy balance:

$$\frac{P_{el,deficit}}{\eta_{shaft}} - c_{p,air}\dot{m}_a T_{inlet,T1}\frac{1-\beta_{T1}^{\varepsilon}}{\eta_{T1}} - c_{p,air}\dot{m}_a T_{inlet,T2}\frac{1-\beta_{T2}^{\varepsilon}}{\eta_{T2}} - c_{p,air}\dot{m}_a T_{inlet,T3}\frac{1-\beta_{T3}^{\varepsilon}}{\eta_{T3}} = 0 \tag{9a}$$

If this balance is satisfied, the algorithm stops and returns the operating point of the turbine train (Fig. 3). Conversely, if this balance is not satisfied, a relaxed closure condition is considered.

$$\frac{P_{el,deficit}}{\eta_{shaft}} > c_{p,air}\dot{m}_a T_{inlet,T1}\frac{1-\beta_{T1}^{\varepsilon}}{\eta_{T1}} + c_{p,air}\dot{m}_a T_{inlet,T2}\frac{1-\beta_{T2}^{\varepsilon}}{\eta_{T2}} + c_{p,air}\dot{m}_a T_{inlet,T3}\frac{1-\beta_{T3}^{\varepsilon}}{\eta_{T3}} \tag{9b}$$

This equation means that the CAES provides a power lower than the residual power load of the district, with the remaining power is

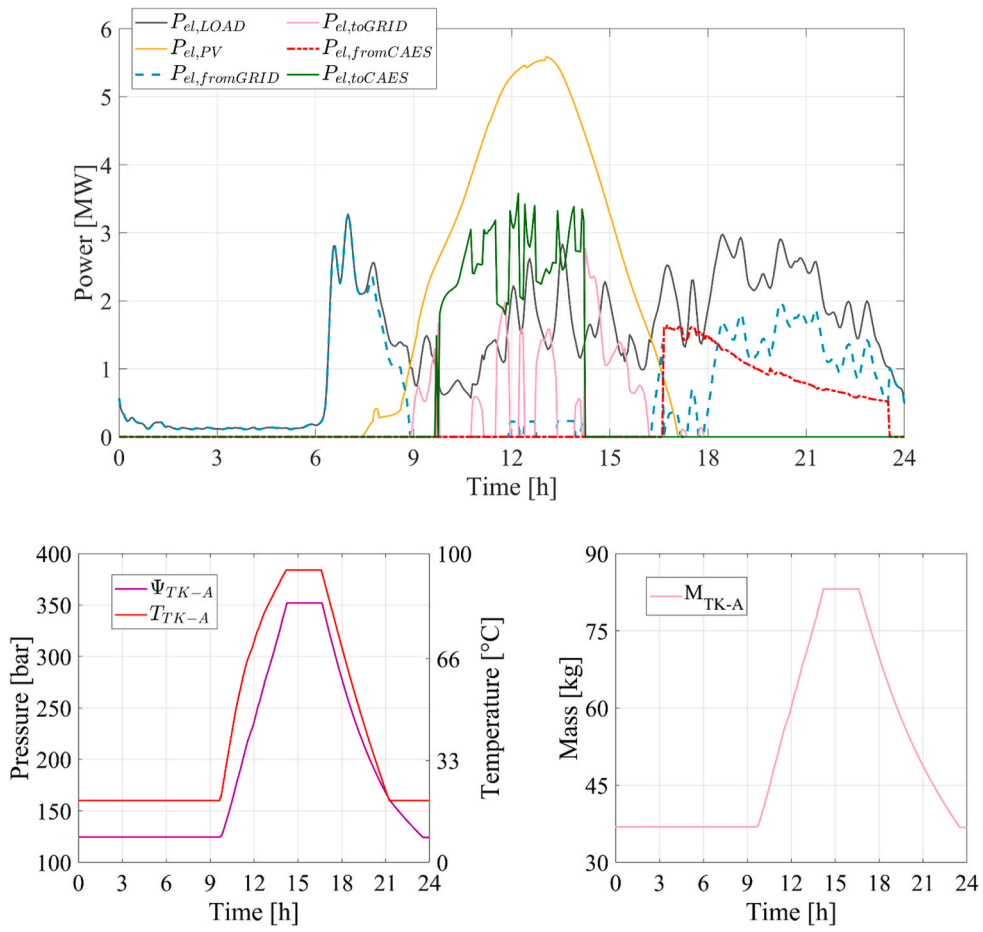

Fig. 7. Dynamic results for a typical winter day: above power results, below tank trends.

withdrawn from the grid, i.e. $P_{el,fromGRID} = P_{el,deficit} - P_{el,fromCAES}$.

If this equation is not satisfied, the algorithm performs all the routines, changing the guessed corrected mass flow rate ($\dot{m}_{c,T1}$Fig. 3). Note that this guess value is still selected from the set of values Λ, Fig. 3.

If the algorithm is unable to find an operating point within the performance maps of the selected turbines that satisfies Eq. (8) or Eq. (9), the turbine train is not activated. This indicates that the given boundary conditions do not allow the turbines to operate. Therefore, the proposed model can identify and discard operating points that fall outside the range of operation for the selected turbines.

Once the operating point for the entire turbine train is assessed, all the previously discussed subroutines are recalled to explicitly determine all the operating parameters of the turbine train. Moreover, the preheating subroutines evaluate the heat exchange occurring in all the preheating heat exchangers (HE-6 to HE-11). Specifically, the outlet temperature of the oil (high-temperature oil ($T_{TK\text{-}OIL\text{-}HT}$) and medium-temperature oil ($T_{TK\text{-}OIL\text{-}MT}$)) is carefully assessed, evaluating the temperature of the oil returning to the oil tanks. Thus, the thermal energy demand of these heat exchangers is thoroughly evaluated. The temperature of the air significantly affects the power provided by the turbine train and the efficiency of the plant.

3.3. Compressed air tank model

The charging phase of a compressed gas tank is featured by an increase in the temperature of the gas stored in the tank. When considering the tank as a control volume, the gas inflow leads to a positive enthalpy flow, which increases the internal energy of the tank (U), causing a rise in the tank temperature (see Eq. (11) and Fig. 4). Conversely, during the discharging phase, the mass flow rate withdrawn from the tank leads to a negative enthalpy flow, reducing the internal energy of the tank (U) causing a decrease in the tank temperature (see Eq. (11) and Fig. 4). These phenomena are well known and analyzed in several works available in the scientific literature (Zhao et al., 2021; Couteau et al., 2022; Li et al., 2022b; Melideo et al., 2017).

Since the temperature of the air in the compressed air tank ($T_{TK\text{-}A}$ see Fig. 1) is a key variable in a CAES plant, the compressed air tank is carefully modelled. According to the literature, the compressed air tank is assumed to be a closed system with only one inlet (charging mode Fig. 4 above) or outlet (discharging mode Fig. 4 below). The governing equations for such a system are summarized by the following systems.

$$\begin{cases} \dfrac{dM}{dt} = \dot{m} \\ \dfrac{dU}{dt} = \dot{m}h \end{cases} \text{charging} \qquad \begin{cases} \dfrac{dM}{dt} = -\dot{m} \\ \dfrac{dU}{dt} = -\dot{m}h \end{cases} \text{discharging} \tag{10}$$

Assuming ideal gas behavior for the air inside the tank, the system of equations can be rearranged as follows.

$$T_{TK-A}(i) = \frac{\left(c_{v,air}/c_{p,air}\right) \cdot T_{TK-A}(i-1) M_{TK-A}(i-1) + T_{feed,a}(i)\dot{m}\Delta t}{M_{TK-A}(i-1) + \dot{m}\Delta t} \tag{11}$$

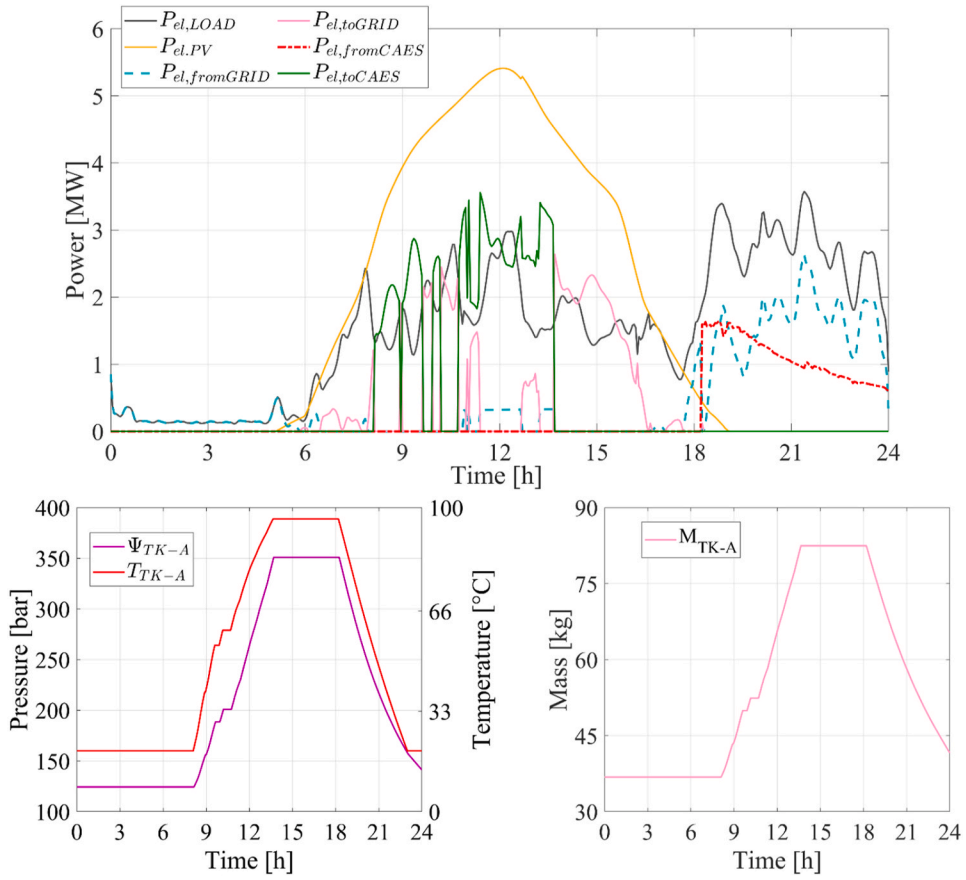

Fig. 8. Dynamic results for a typical summer day: above power results, below tank trends.

$$T_{TK-A}(i) = \frac{(c_{v,air}/c_{p,air}) \cdot T_{TK-A}(i-1) M_{TK-A}(i-1) - T_{withdrawn,a}(i-1)\dot{m}\Delta t}{M_{TK-A}(i-1) - \dot{m}\Delta t} \tag{12}$$

At each time step (Δt), eq. (11) allows one to evaluate the temperature inside the tank (T_{TKa}(i)) during the charging phase (see Fig. 4 below), while eq. (12) assesses the temperature inside the tank (T_{TKa}(i)) during the discharging phase (see Fig. 4 below). M_{TK-A} represents the mass of gas stored into the tank.

The tank is also equipped with a heat exchanger designed to heat the tank during the discharging phase when the temperature of the tank decreases. As described in the *System Layout* section (Fig. 1), the heat exchanger is only activated when the tank temperature (T_{TK-A}) drops to 20 °C.

When the tank temperature approaches 20 °C, the water is delivered to the heat exchanger installed on the air tank. The temperature of the tank is evaluated according to the following system of equations.

$$\begin{cases} \dot{m}c_{v,air}T_{TK-A}(i) = \dot{m}c_{p,air}T_{TK-A}(i) + UA\ln\left[\dfrac{\left(T_{w,in}(i) - T_{TK-A}(i)\right) - \left(T_{w,out}(i) - T_{TK-A}(i)\right)}{\ln\left[\left(T_{w,in}(i) - T_{TK-A}(i)\right)/\left(T_{w,out}(i) - T_{TK-A}(i)\right)\right]}\right] \\ UA\ln\left[\dfrac{\left(T_{w,in}(i) - T_{TK-A}(i)\right) - \left(T_{w,out}(i) - T_{TK-A}(i)\right)}{\ln\left[\left(T_{w,in}(i) - T_{TK-A}(i)\right)/\left(T_{w,out}(i) - T_{TK-A}(i)\right)\right]}\right] - \dot{m}_w c_{p,water}\left[T_{w,in}(i) - T_{w,out}(i)\right] = 0 \end{cases} \tag{13}$$

This system of equations represents the energy balance for the compressed air tank and the heat exchanger installed on the tank. The heat exchange phenomena are modelled using the logarithmic mean temperature difference approach (Stewart and Stewart, 2014). Note that the results returned by such model are validated against the ones returned by the software Refprop (Lemmon et al., 2007).

3.4. Thermoeconomic model

The energy performance of the proposed system (see System Layout) and of the reference system (RS) are evaluated according to the following equations.

$$PE_{RS} = \frac{E_{el,fromGRID,RS}}{\eta_{el}} \tag{14a}$$

$$PE_{PS} = \frac{E_{el,fromGRID,PS} - E_{el,toGRID}}{\eta_{el}} \tag{14b}$$

$$PES = \frac{PE_{RS} - PE_{PS}}{PE_{RS}} \tag{14c}$$

Where $E_{el,fromGRID}$ represents the electricity withdrawn from the grid, and $E_{el,toGRID}$ the electricity delivered to the grid. Both the reference and the proposed system are fully electric users, which will be clearly

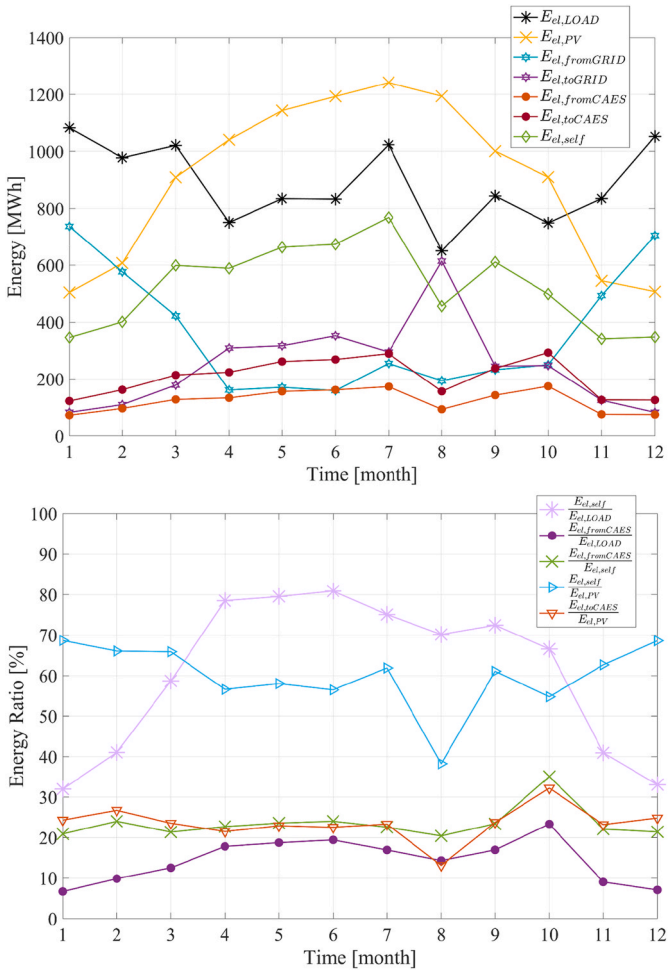

Fig. 9. Monthly results: electricity performance. Above electricity flux. Below electric energy ratios.

discussed in the *Case Study* section.

The economic performances are assessed as follows.

$$C_{RS} = j_{el,fromGRID} E_{el,fromGRID,RS} \tag{15a}$$

$$C_{PS} = j_{el,fromGRID} E_{el,fromGRID,PS} - j_{el,toGRID} E_{el,toGRID} \tag{15b}$$

$$\Delta C = \frac{C_{RS} - C_{PS}}{C_{RS}} \tag{15c}$$

$$SPB = \frac{C_{tot}}{\Delta C} \tag{15d}$$

Where the investment cost of the proposed system is evaluated according to the following equation.

$$C_{tot} = J_{Cs} + J_{Ts} + J_{CH} + J_{CT} + J_{pumps} + J_{TKs} + J_{TKA} + J_{HEs} + J_{ETC} + J_{PV} \tag{16}$$

Note that Table 1Table 1 in detail reports all the cost figures.

Finally, the following parameters are calculated in order to better analyze the performance of the proposed plant. R_{renew} represents the share of the user load matched by means of renewable electricity.

$$R_{renew} = 1 - \frac{E_{el,fromGRID,PS}}{E_{el,fromGRID,RS}} \tag{17}$$

The performance of the CAES is assessed by means of the average efficiency of the compressors train ($\eta_{C,average}$) the average efficiency of the turbines train ($\eta_{T,average}$) and the round-trip efficiency ($\eta_{roundtrip}$).

$$\eta_{C,average} = \frac{P_{C1,iso}/\eta_{C1} + P_{C2,iso}/\eta_{C2} + P_{C3,iso}/\eta_{C3}}{P_{el,available}} \tag{18a}$$

$$\eta_{T,average} = \frac{P_{T1,iso}/\eta_{T1} + P_{T2,iso}/\eta_{T2} + P_{T2,iso}/\eta_{T2}}{P_{el,produced}} \tag{18b}$$

$$\eta_{roundtrip} = \frac{E_{el,fromCAES}}{E_{el,toCAE}S + E_{el,toCH} + E_{el,toCT}} \tag{19a}$$

$$\eta_{roundtrip,overall} = \frac{E_{el,fromCAES}}{E_{el,toCAE}S + E_{el,toCH} + E_{el,toCT} + E_{\mathrm{th},sol}} \tag{19b}$$

Where, $P_{Ci,iso}$ and $P_{Ti,iso}$ are the compressor and turbine isentropic power, respectively. $E_{el,fromCAES}$ is the electricity delivered from the CAES to the residential district, $E_{el,toCAES}$ is the electricity delivered to the CAES, $E_{el,toCH}$ and $E_{el,toCT}$ are the electricity supplied to the electric chiller and to the cooling tower for cooling the cooling circuit of the CAES.

4. Case study

The proposed renewable plant is designed to serve a residential district, consisting of 50 buildings, and located in Naples, Southern Italy. The main features regarding such district are available in Ref. (Calise et al., 2020, 2023a, 2024). For detailed information on the methodology used for collecting the data needed to model this district, refer to Ref (Calise et al., 2020). For brevity, only a brief description of the district is here provided. The selected residential district includes buildings that were built during the same era, so they are assumed to have similar thermophysical properties, see Table 2 (Calise et al., 2020). The selected residential district is considered to be fully electric, where the space heating and cooling demands are met by independent air-to-air heat pumps. The thermal energy demand for domestic hot water (DHW) is met by an air-to-water heat pump (ANK-050 Aermec) (Calise et al., 2023a).

The reference system (RS) consists of the fully electric residential district described above, where the power demand is met by electricity withdrawn from the grid.

The proposed system (PS) integrates this residential district with a 6.30 MW PV field and an AA-CAES system designed to shave the peaks of the district power demand and renewable power production. This AA-CAES plant is designed to increase the residential district self-sufficiency.

The CAES system includes a train of three intercooled compressors, with a total capacity of 3.50 MW. The first two compressors are centrifugal compressors, obtained by scaling the map of the ASME 95-GT-79 (Figaj, 2021; Xu et al., 2021; Calise et al., 2007; Wang et al., 2017) compressor according to the required plant capacity. The third compressor is a piston compressor. Fig. 5 displays the performance map of the scaled compressors C1 and C2 included into the compressors train.

The CAES includes a train of interheated turbines, with a rated capacity of 1.50 MW. The turbines of such trains are designed by scaling the map of the radial turbine NASA-CR-174646 (Mehigan et al., 2022; Calise et al., 2007, 2019a) according to the plant requirement. Fig. 6 shows the maps of the scaled turbines.

Table 3 lists the main design data for the main components included in the proposed layout, namely: PV field, evacuated tube collectors (ETC), heat exchangers, compressors, turbines, chiller, and tanks. The size of the oil and water tanks were properly designed to maximize thermal energy storage. In particular, such tanks are capable of storing nearly 4 h of waste heat generated by the compressors. The PV fields and the ETC are designed with a very high capacity with the aim of maximizing the contribution of renewable solar energy. The compressed air tank is featured by a maximum pressure of 350 bar and a volume of 250 m^3, being able to store almost 7.00–9.00 MWh of energy in terming of electric energy.

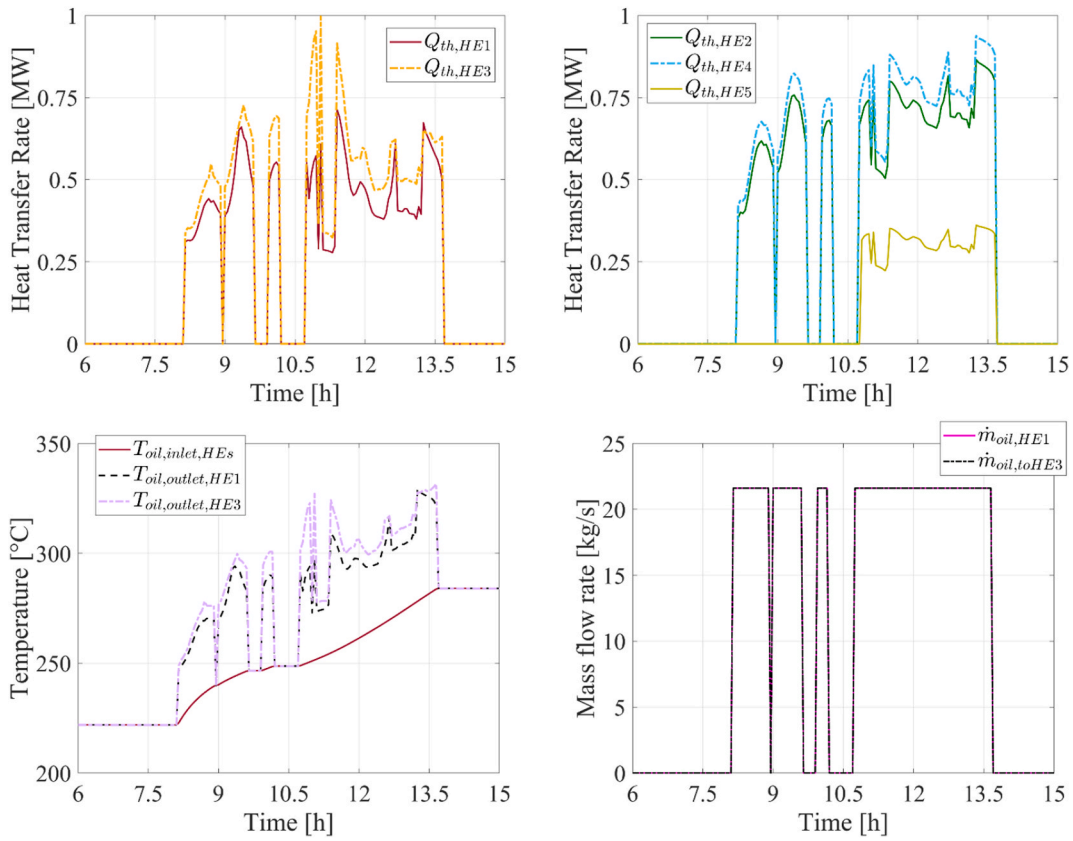

Fig. 10. Compressors dynamic performance: above heat transfer rate below hot oil loop results.

5. Results

This section presents the results achieved by the proposed model of a residential district integrated with a 6.30 MW photovoltaic (PV) system and a compressed air energy storage (CAES) of approximately 7.00–9.00 MWh. The simulation was performed using a PC equipped with an *AMD Ryzen 7 5700G* (3.80 GHz) as CPU and a 16.0 GB RAM. Each single simulation takes about 30–40 h.

5.1. Overall system performance

The proposed system achieves promising energy results with a renewable energy factor (R_{renew} eq. (16)) of 59 % (Table 4). This is mainly due to the high self-consumption of renewable electricity ($E_{el,self}$), which meets nearly 59 % of the residential district electricity demand ($E_{el,LOAD}$), accounting for roughly 6.30 GWh/y, as shown in Table 4. The CAES system plays a crucial role in enhancing the share of self-consumed energy. In fact, the CAES provides about 1.48 GWh/y, meeting 14 % of the district annual demand (see $E_{el,fromCAES}/E_{el,LOAD}$ in Table 4) and contributing by 24 % to the self-consumed energy ($E_{el,fromCAES}/E_{el,self}$, see in Table 4). Despite these trends, the excess electricity not used by the district and exported to the grid ($E_{el,toGRID}/E_{el,PV}$ in Table 4) accounts for 27 % of the produced renewable photovoltaic electricity ($E_{el,PV}$).

Figs. 7 and 8 clearly justify such results. During the central part of the day, when the PV power production ($P_{el,PV}$) exceeds the residential district power demand ($P_{el,LOAD}$), the excess electricity is used to activate the CAES system ($P_{el,toCAES}$), i.e., the compressors, storing the electricity as compressed air (Figs. 7 and 8). From 09:00 to 13:00, nearly 3.20 MW of power is delivered to the compressors ($P_{el,toCAES}$), both for typical winter and summer days (Figs. 7 and 8). The tank pressure (ψ) reaches the maximum allowed value of 350 bar around 13:00, enabling the system to store surplus electricity for nearly 4 h. During the charging phase, the tank temperature increases due to the positive enthalpy flow associated with the mass flow rate delivered to the tank (Figs. 7 and 8).

The electricity used to run the compressors significantly fluctuates. Sometimes, the excess electricity is delivered to the grid ($P_{el,toGRID}$) instead of the compressors, even if the tank is not fully charged. When the tank pressure increases, the minimum power needed to activate the compressors also increases due to the higher overall compression ratio and the corresponding increase in work required by the compressors. This aspect highlights that the model can discard operating points that fall outside the compressors performance maps. Moreover, this result clearly remarks that the main challenge regarding the CAES relies on the management of the compressors. The compressors are featured by a limited range of operation. For this reason, the compressors significantly limit the flexibility of such a system. Nonetheless, the CAES system effectively smooths the peaks of surplus electricity, Figs. 7 and 8.

In the evening, starting from 17:00, the turbines are activated to meet part of the $P_{el,LOAD}$ (Figs. 7 and 8). The power supplied by the turbines ($P_{el,fromCAES}$) decreases as the tank pressure drops (Figs. 7 and 8). As the tank pressure decreases, the enthalpy of the compressed air at the turbines inlets also decreases, reducing the generated electricity. Unlike the compressors, the turbines operate continuously, providing all the power they can to meet a certain amount of the load (see $P_{el,fromCAES}$ Figs. 7 and 8). The power load ($P_{el,LOAD}$) never falls below the minimum power produced by the turbines. The turbines provide power ranging from 1.50 MW to 0.70 MW (Figs. 7 and 8). During the tank discharge, the tank temperature decreases due to the emptying process (Figs. 7 and 8).

A seasonal trend is clearly detected: as PV electricity production increases, the self-consumed energy also rises (Fig. 9). From April to July, self-consumed energy meets around 75 % of the residential district load (see $E_{el,self}/E_{el,LOAD}$ in Fig. 9). In August, an increase in excess electricity ($E_{el,toGRID}$) is observed, due to high PV production ($E_{el,PV}$ equal to 1200 MWh/month) and reduced load, as most residents are on

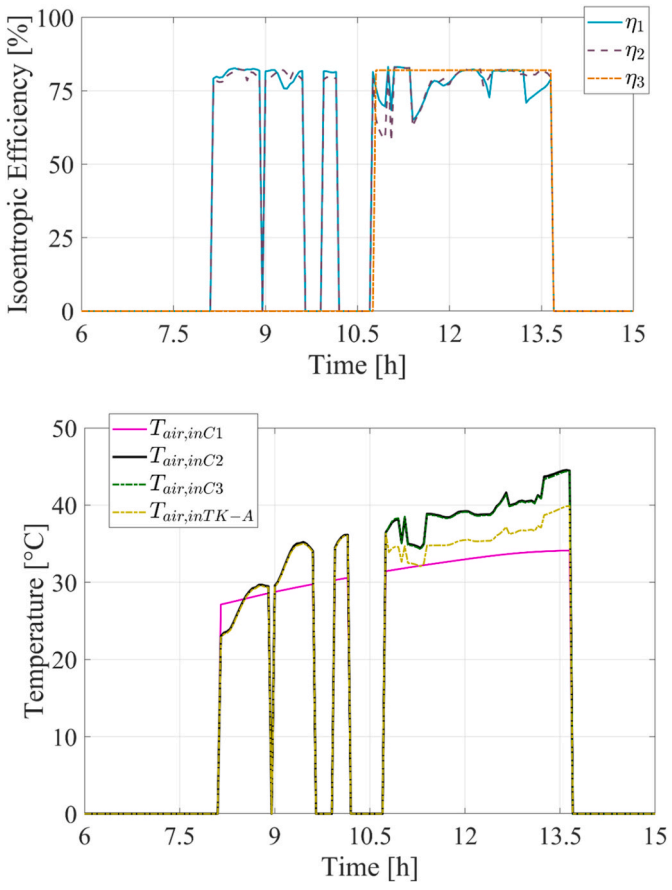

Fig. 11. Compressors train dynamic results: above efficiency of the single compressors and average efficiency of the compressors train, below temperature at the inlet of the compressors.

vacation.

From an economic perspective, the system yields moderate results. It reduces the district operating costs by 53 %, from 3.20 M€/year to 1.52 M€/year. However, the Simple Payback Period (*SPB*) is significantly high, at 21.3 years, mainly due to the high capital cost of some components such as turbines and compressors, which account for 66 % of the total investment cost.

5.2. Compressed air energy storage performance

The performance of a CAES system in terms of electric energy storage and provision deeply depends on the thermal management of the entire plant. The thermal energy recovered from the compressors, exploited for driving the turbines ($E_{th,O\text{-}HT,toTs}$), accounts for 1.01 GWh/y, matching almost 54 % of the thermal energy supplied to the turbines (see ratio $E_{th,O\text{-}HT,toTs}/E_{th,Ts}$ in Table 4). Moreover, the system is able to utilize almost 47 % of the waste heat from the compression work (see the ratio $E_{th,O\text{-}HT,toTs}/E_{th,Cs}$ in Table 4). This result is mainly due to the proposed plant reliance on two cooling loops: an oil-driven cooling loop and a water-driven cooling loop (see Fig. 1 in *System Layout* section). The oil-driven cooling loop is designed to maximize the temperature of the oil exiting the heat exchangers (HE-1 and HE-3 Fig. 1). This oil is used to increase the temperature, i.e., the enthalpy, of the air at the inlet of the turbines. The water-driven loop is designed to cool the air at the compressors inlet close to ambient temperature (HE-2, HE-4, and HE-5 in Fig. 1). According to Fig. 10, on average, 50 % of the waste heat is discharged into the oil loop (see $Q_{th,HE1}$ and $Q_{th,HE3}$), and 50 % into the water loop (see $Q_{th,HE2}$, $Q_{th,HE4}$ and $Q_{th,HE5}$). The heat transfer rate discharged into both loops is roughly 1.60 MW each (Fig. 10). Note that the $T_{oil,\ inlet,HEs}$ refers to the diathermic oil temperature at the feeding side of the both oil driven heat exchangers HE1 and HE3.

As noted, these heat exchanges succeed in limiting the temperature at the compressors inlet (Fig. 11). This results in a very high efficiency of the compressors, with all compressors operating at around 80.0 ± 2.5 % isentropic efficiency, and the overall average isentropic efficiency of the compression train reaching almost 81.0 ± 3.0 %. These values are obtained from the compressors performance map, depending on the time dependent boundary condition, i.e. the available power and the coolant fluids temperature. These trends mimic the real operation of the selected compressor under off-design conditions.

The fluctuating trend observed for the compressors is due to the increasing pressure inside the tank, which raises the minimum power needed to activate the entire compression train. This point is discussed in the previous section. The temperature at the compressors inlet rises because the coolant fluids temperature increases during operation, due to the heat discharged by the compressors.

The thermal energy recovered and stored into the high temperature oil loop (tank TK-O-HT) is used for heating the air before it enters the turbines. The air entering the turbines is preheated by solar oil (medium temperature oil) and further heated by high-temperature oil heated by the compressors waste heat. Both loops, high-temperature and medium-temperature, contribute almost equally to heating the air before it enters the turbines, with medium temperature oil providing 47 % of the thermal energy delivered to the turbines (see $E_{th,O\text{-}MT,toTs}/E_{th,Ts}$ in Table 4) and high-temperature oil providing 53 % of the thermal energy supplied to the turbines (see $E_{th,O\text{-}HT,toTs}/E_{th,Ts}$ in Table 4). This heating process is crucial for increasing the enthalpy of the air entering the turbines, thereby enhancing turbine efficiency.

Fig. 12 is consistent with these trends, showing that medium temperature oil provides about 1.20 MW, and hot oil also provides about

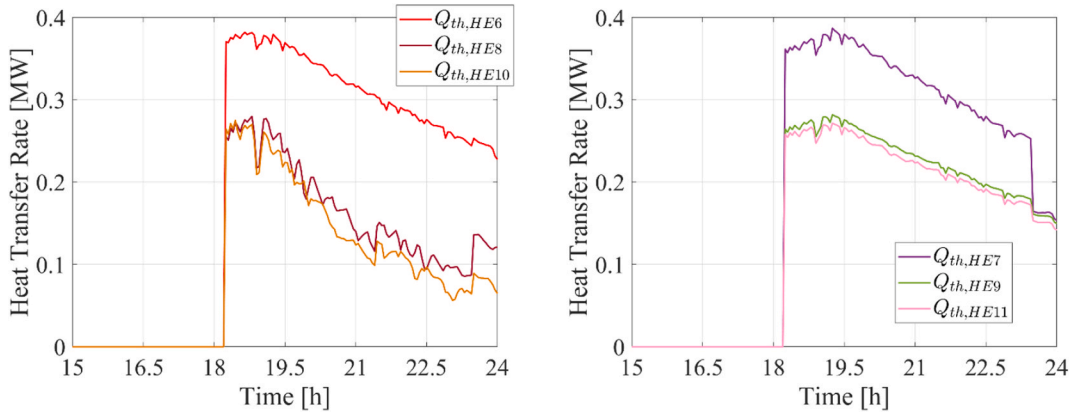

Fig. 12. Turbine train dynamic results: heat transfer rates.

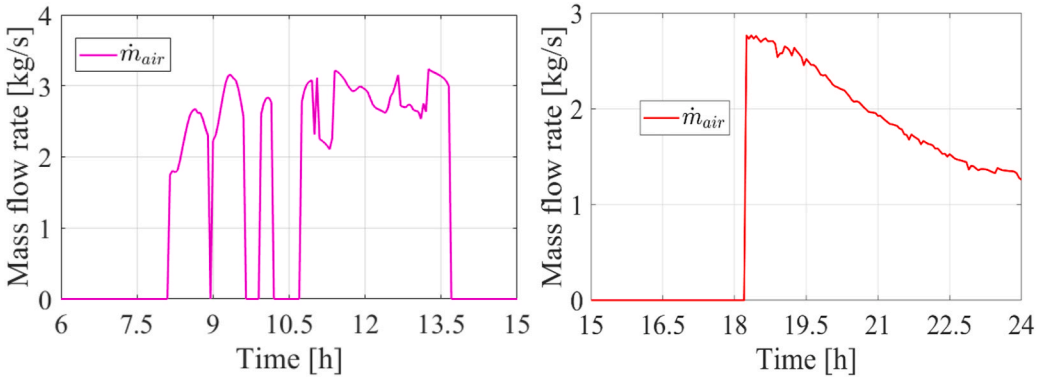

Fig. 13. Dynamic mass flow rate of the compressor train (left) and turbine train (right).

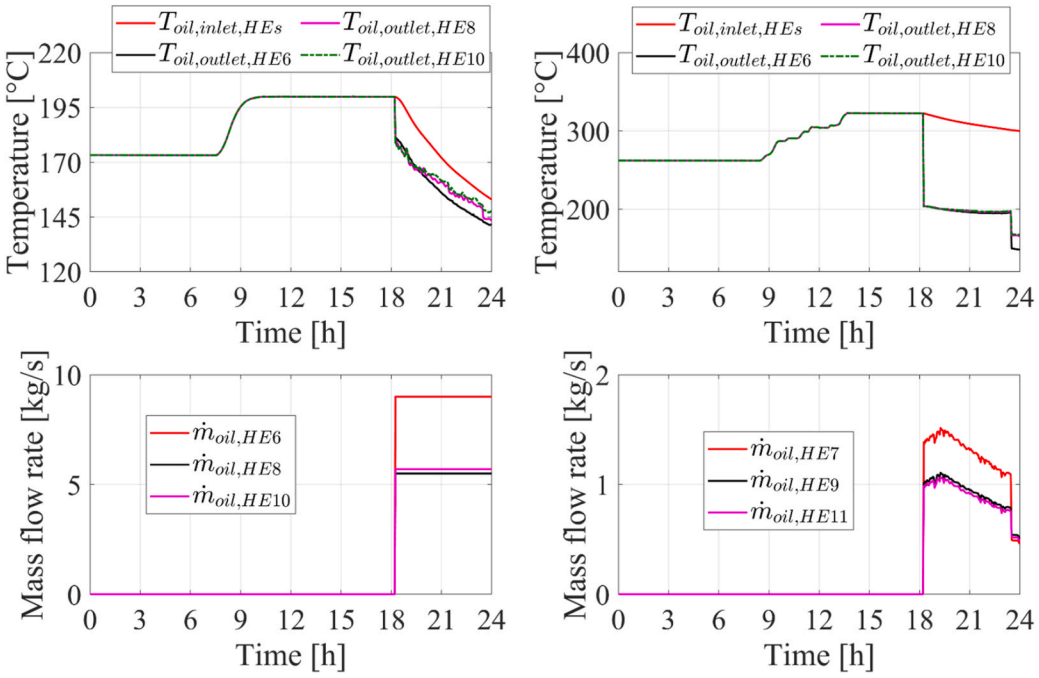

Fig. 14. Turbine train dynamic results: heating system dynamic performance.

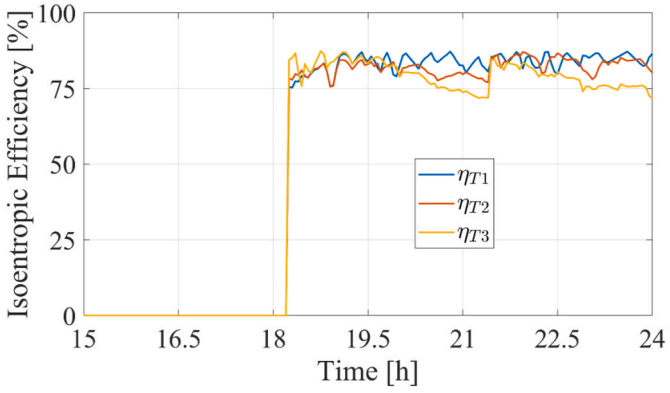

Fig. 15. Turbines train dynamic results: efficiency of the single turbine.

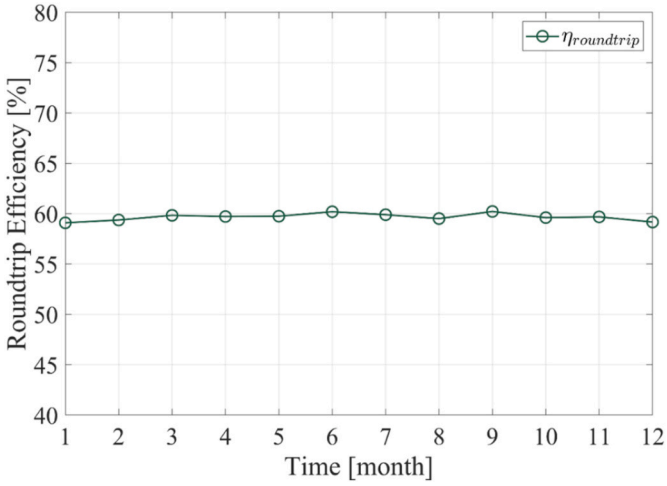

Fig. 16. Monthly round-trip efficiency.

1.20 MW. The heat provided by both loops decreases as the mass flow rate of air to the turbines decreases when the tank pressure drops (Fig. 13). Fig. 14 summarizes the heating system performance, showing that the plant maintains the air temperature at the turbines inlet at

280 °C. As described in the *System Layout* section, this system is managed by a feedback controller that selects the proper oil mass flow rate to achieve an inlet air temperature of 280 °C. This system is crucial for ensuring the turbines operate at their highest efficiency, with the turbines train achieving an overall efficiency of around 80.0 ± 2.5 % (see Fig. 15).

The high isentropic efficiency of the turbine and compressor trains is crucial for improving the system round-trip efficiency. The proposed CAES system round-trip efficiency, assessed according to eq. (19), is 59 % annually (Table 4). However, this value shows a seasonal trend. During the summer months, when solar availability is higher, the round-trip efficiency reaches 61 %. Conversely, in winter, it drops to 59 % (Fig. 16). This is because, in summer, the available power is greater, allowing the compressors to operate under more favorable conditions according to their performance map.

6. Conclusions

The proposed research presents a co-simulation model for simulating the time dependent performance of a renewable plant equipped with a compressed air energy storage system driven by renewables. In particular, such paper provides a completely novel model for mimicking the off-design performance of a compressed air energy storage system, based on the performance map approach. In addition, the proposed model also includes a proper compressed air tank model, taking into account the temperature rise/decrease in charging/discharging phase. The simulation model of the compressors train, turbines trains and compressed air tank are developed in MATLAB. These models are connected to the renewable plant and users developed in TRNSYS by means of the type 155. Note that the provided model pays particular attention to the heat exchange phenomena occurring in the developed plant. In fact, this plant is also equipped with a waste heat management system for recovering the waste heat during the compression phase to reduce the temperature of the air at the inlet of each compressor. Such heat is used for preheating the compressed air delivered to the turbines, increasing the air enthalpy at the inlet of the turbines.

This plant is designed for operating as electric energy storage system to shave the peak of power demand and power production of a residential district, equipped with a renewable power plant. The selected user is a residential district, including 50 buildings located in Naples, southern Italy. Such district is supposed to be fully electric: the energy for building space heating and cooling are met by means of reversible air-to-air heat pumps, the domestic hot water is produced by means of individual air-to-water heat pumps. Thus, the electricity withdrawn from the grid balances the district load, also including the electricity for running heat pumps.

The proposed system includes a photovoltaic field of 6.30 MW a compressor train of rated capacity of 3.5 MW a turbine train of rated capacity of 1.5 MW and a tank of 250 m^3 and 350 bar. The compressors train includes two centrifugal compressors and one piston compressor. The turbines train includes three radial turbines. Moreover, to further increase the thermal energy delivered to the turbines such plant also includes an evacuated collector field of 2000 m^2, i.e. 1.30 MW at rated conditions. The main results achieved by this research are summarized below.

- The proposed plant reduces the primary energy consumption of the considered residential district by nearly 60 %.
- The compressed air energy storage system plays a crucial role in increasing the district self-consumption, in fact it accounts for 23 % of the self-consumed energy, meeting 13 % of district load.
- The evacuated collectors solar field provides almost 50 % of the thermal energy delivered to the turbines.
- The system achieves a quite high round trip efficiency, i.e. 59 %. This result is mainly due to the waste heat management system. The proposed system succeeds in limiting the temperature at the compressors inlet and at the same time such system is able to steer the temperature of the air at the inlet of the turbines. For these reasons turbines and compressors operate with high isentropic efficiency.
- The proposed plant achieves poor economic performance, i.e. a payback period of almost 21 years, because the high capital cost of the technologies involved.

The proposed layout successfully simulates the time dependent off-design performance of the proposed compressed air energy storage system. In particular such research highlights that the main limitation of a compressed air energy storage system is the compressors train. In fact, the compressors are featured by a very limited operation domain. In other words, the compressors features limit the flexibility of a compressed air energy storage system. Further analyses should be performed in order to study if other compressor technology could better suit the operation of a compressed air energy storage system.

CRediT authorship contribution statement

Francesco Calise: Writing – review & editing, Supervision, Funding acquisition, Conceptualization. **Francesco Liberato Cappiello:** Writing – review & editing, Writing – original draft, Visualization, Validation, Supervision, Software, Resources, Project administration, Methodology, Investigation, Funding acquisition, Formal analysis, Data curation, Conceptualization. **Luca Cimmino:** Writing – review & editing, Writing – original draft, Visualization, Data curation. **Maria Vicidomini:** Writing – original draft, Visualization, Data curation.

Declaration of competing interest

The corresponding author confirms that no ethical issues and conflict of interest are involved. In particular the author confirms that he has no known competing financial interests or personal relationships that could have appeared to influence the work reported in this paper.

Acknowledgement

The authors gratefully acknowledge the partial financial support of the project “Sustainable Energy Networks” CUP E65F21003190003.

Project funded under the National Recovery and Resilience Plan (NRRP), Mission 4, Component 2, Investment 1.3 - Call for tender No. 1561 of October 11, 2022 of Ministero dell’Università e della Ricerca (MUR); funded by the European Union – NextGenerationEU• Award Number: Project code PE0000021, Concession Decree No. 1561 of October 11, 2022 adopted by Ministero dell’Università e della Ricerca (MUR), CUP E63C22002160007, Project title: “Network 4 Energy Sustainable Transition – NEST”

Data availability

Data will be made available on request.

References

Abe, Y., Watanabe, R., Yodose, T., Kumagai, S., 2024. Cathode active materials using rare metals recovered from waste lithium-ion batteries: a review. Heliyon 10, e28145.

Ahamed, M.S., Guo, H., Tanino, K., 2020. Modeling heating demands in a Chinese-style solar greenhouse using the transient building energy simulation model TRNSYS. J. Build. Eng. 29, 101114.

Air Liquide - https://it.airliquide.com/.

Alirahmi, S.M., Bashiri Mousavi, S., Razmi, A.R., Ahmadi, P., 2021. A comprehensive techno-economic analysis and multi-criteria optimization of a compressed air energy storage (CAES) hybridized with solar and desalination units. Energy Convers. Manag. 236, 114053.

Angrisani, G., Rosato, A., Roselli, C., Sasso, M., Sibilio, S., Unich, A., 2014. Influence of climatic conditions and control logic on NOx and CO emissions of a micro-cogeneration unit serving an Italian residential building. Appl. Therm. Eng. 71, 858–871.

Ardizzon, G., Cavazzini, G., Pavesi, G., 2014. A new generation of small hydro and pumped-hydro power plants: advances and future challenges. Renew. Sustain. Energy Rev. 31, 746–761.
Assareh, E., Ghafouri, A., 2023. An innovative compressed air energy storage (CAES) using hydrogen energy integrated with geothermal and solar energy technologies: a comprehensive techno-economic analysis - different climate areas- using artificial intelligent (AI). Int. J. Hydrogen Energy 48, 12600–12621.
Baqari, F., Vahidi, B., 2013. Small-compressed air energy storage system integrated with induction generator for metropolises: a case study. Renew. Sustain. Energy Rev. 21, 365–370.
Bazdar, E., Sameti, M., Nasiri, F., Haghighat, F., 2022. Compressed air energy storage in integrated energy systems: a review. Renew. Sustain. Energy Rev. 167, 112701.
BellissMorcom - https://www.bellissandmorcom.com/en-us/.
Bertini, M., Fiaschi, D., Manfrida, G., H Niknam, P., Talluri, L., 2021. Evaluation of the property methods for pure and mixture of CO2 for power cycles analysis. Energy Convers. Manag. 245, 114568.
Bibra, E.M., Connelly, E., Dhir, S., Drtil, M., Henriot, P., Hwang, I., et al., 2022. Global EV Outlook 2022: Securing Supplies for an Electric Future.
Böhm, H., Zauner, A., Rosenfeld, D.C., Tichler, R., 2020. Projecting cost development for future large-scale power-to-gas implementations by scaling effects. Appl. Energy 264, 114780.
Bordignon, S., Emmi, G., Zarrella, A., De Carli, M., 2021. Energy analysis of different configurations for a reversible ground source heat pump using a new flexible TRNSYS Type. Appl. Therm. Eng. 197, 117413.
Boyce, M.P., 2012. 7 - axial-flow compressors. In: Boyce, M.P. (Ed.), Gas Turbine Engineering Handbook, fourth ed. Butterworth-Heinemann, Oxford, pp. 303–355.
M.P. Boyce. 2 - advanced industrial gas turbines for power generation. in: A.D. Rao, (Ed.). Combined Cycle Systems for Near-Zero Emission Power Generation. Woodhead Publishing2012. pp. 44-102.
Budt, M., Wolf, D., Span, R., Yan, J., 2016. A review on compressed air energy storage: basic principles, past milestones and recent developments. Appl. Energy 170, 250–268.
Burckhardt Compression - https://www.burckhardtcompression.com/solution/h2-power-to-x-mobility/h2-liquefaction/.
Calise, F., Dentice d' Accadia, M., Vanoli, L., von Spakovsky, M.R., 2007. Full load synthesis/design optimization of a hybrid SOFC–GT power plant. Energy 32, 446–458.
Calise, F., Dentice d'Accadia, M., Piacentino, A., 2014. A novel solar trigeneration system integrating PVT (photovoltaic/thermal collectors) and SW (seawater) desalination: dynamic simulation and economic assessment. Energy 67, 129–148.
Calise, F., Cappiello, F.L., Cartenì, A., Dentice d'Accadia, M., Vicidomini, M., 2019a. A novel paradigm for a sustainable mobility based on electric vehicles, photovoltaic panels and electric energy storage systems: case studies for Naples and Salerno (Italy). Renew. Sustain. Energy Rev. 111, 97–114.
Calise, F., Dentice d'Accadia, M., Vanoli, R., Vicidomini, M., 2019b. Transient analysis of solar polygeneration systems including seawater desalination: a comparison between linear Fresnel and evacuated solar collectors. Energy 172, 647–660.
Calise, F., Cappiello, F.L., Dentice d'Accadia, M., Vicidomini, M., 2020. Energy efficiency in small districts: dynamic simulation and technoeconomic analysis. Energy Convers. Manag. 220, 113022.
Calise, F., Cappiello, F.L., Dentice d'Accadia, M., Vicidomini, M., 2021a. Thermo-economic optimization of a novel hybrid renewable trigeneration plant. Renew. Energy 175, 532–549.
Calise, F., Cappiello, F.L., Dentice d'Accadia, M., Vicidomini, M., 2021b. Smart grid energy district based on the integration of electric vehicles and combined heat and power generation. Energy Convers. Manag. 234, 113932.
Calise, F., Cappiello, F.L., Cimmino, L., Vicidomini, M., 2022. Dynamic simulation modelling of reversible solid oxide fuel cells for energy storage purpose. Energy 260, 124893.
Calise, F., Cappiello, F.L., Cimmino, L., Dentice d'Accadia, M., Vicidomini, M., 2023a. Renewable smart energy network: a thermoeconomic comparison between conventional lithium-ion batteries and reversible solid oxide fuel cells. Renew. Energy 214, 74–95. https://doi.org/10.1016/j.renene.2023.05.090.
Calise, F., Cappiello, F.L., Cimmino, L., Dentice d'Accadia, M., Vicidomini, M., 2023b. Renewable smart energy network: a thermoeconomic comparison between conventional lithium-ion batteries and reversible solid oxide fuel cells. Renew. Energy 214, 74–95.
Calise, F., Cappiello, F.L., Cimmino, L., Dentice d'Accadia, M., Vicidomini, M., 2024. Thermo-economic analysis and dynamic simulation of a novel layout of a renewable energy community for an existing residential district in Italy. Energy Convers. Manag. 313, 118582.
Cappiello, F.L., Erhart, T.G., 2021. Modular cogeneration for hospitals: a novel control strategy and optimal design. Energy Convers. Manag. 237, 114131.
Çengel, Y.A., 2009. Termodinamica e trasmissione del calore. McGraw-Hill Companies.
Chen, H., Peng, Y.-h., Wang, Y.-l., Zhang, J., 2020a. Thermodynamic analysis of an open type isothermal compressed air energy storage system based on hydraulic pump/turbine and spray cooling. Energy Convers. Manag. 204, 112293.
Chen, S., Rahbari, H.R., Arabkoohsar, A., Zhu, T., 2020b. Impacts of partial-load service on energy, exergy, environmental and economic performances of low-temperature compressed air energy storage system. J. Energy Storage 32, 101900.
Copco, A., 2024. https://www.atlascopco.com/.
Courtois, N., Najafiyazdi, M., Lotfalian, R., Boudreault, R., Picard, M., 2021. Analytical expression for the evaluation of multi-stage adiabatic-compressed air energy storage (A-CAES) systems cycle efficiency. Appl. Energy 288, 116592.
Couteau, A., Dimopoulos Eggenschwiler, P., Jenny, P., 2022. Heat transfer analysis of high pressure hydrogen tank fillings. Int. J. Hydrogen Energy 47, 23060–23069.
Dib, G., Haberschill, P., Rullière, R., Revellin, R., 2021. Thermodynamic investigation of quasi-isothermal air compression/expansion for energy storage. Energy Convers. Manag. 235, 114027.
Ding, H., Dong, Y., Zhang, Y., Wen, C., Yang, Y., 2024. Performance of supercritical carbon dioxide (sCO2) centrifugal compressors in the Brayton cycle considering non-equilibrium condensation and exergy efficiency. Energy Convers. Manag. 299, 117849.
Diyoke, C., Wu, C., 2020. Thermodynamic analysis of hybrid adiabatic compressed air energy storage system and biomass gasification storage (A-CAES + BMGS) power system. Fuel 271, 117572.
Du, R., He, Y., Chen, H., Xu, Y., Li, W., Deng, J., 2022. Performance and economy of trigenerative adiabatic compressed air energy storage system based on multi-parameter analysis. Energy 238, 121695.
E. Comission. https://energy.ec.europa.eu/topics/energy-systems-integration/hydrogen/renewable-hydrogen_en#:~:text=Renewable%20hydrogen%20is%20promoted%20in,June%202023%20two%20delegated%20acts.
Fan, T., Liang, W., Guo, W., Feng, T., Li, W., 2023. Life cycle assessment of electric vehicles' lithium-ion batteries reused for energy storage. J. Energy Storage 71, 108126.
Fei, Z., Su, Y., Zha, Y., Zhao, X., Meng, Q., Dong, P., et al., 2023. Selective lithium extraction of cathode materials from spent lithium-ion batteries via low-valent salt assisted roasting. Chem. Eng. J. 464, 142534.
Figaj, R., 2021. Performance assessment of a renewable micro-scale trigeneration system based on biomass steam cycle, wind turbine, photovoltaic field. Renew. Energy 177, 193–208.
Flexer, V., Baspineiro, C.F., Galli, C.I., 2018. Lithium recovery from brines: a vital raw material for green energies with a potential environmental impact in its mining and processing. Sci. Total Environ. 639, 1188–1204.
Gasanzade, F., Witte, F., Tuschy, I., Bauer, S., 2023. Integration of geological compressed air energy storage into future energy supply systems dominated by renewable power sources. Energy Convers. Manag. 277, 116643.
Ghalelou, A.N., Fakhri, A.P., Nojavan, S., Majidi, M., Hatami, H., 2016. A stochastic self-scheduling program for compressed air energy storage (CAES) of renewable energy sources (RESs) based on a demand response mechanism. Energy Convers. Manag. 120, 388–396.
Giampaolo, A., 2020. Compressor Handbook: Principles and Practice. CRC Press.
Guo, H., Xu, Y., Guo, C., Zhang, Y., Hou, H., Chen, H., 2019. Off-design performance of CAES systems with low-temperature thermal storage under optimized operation strategy. J. Energy Storage 24, 100787.
Hai, T., Zoghi, M., Javaherdeh, K., 2023. 4E analysis and optimization of a biomass-fired waste-to-energy plant integrated with a compressed air energy storage system for the multi-generation purpose. Fuel 348, 128457.
Han, Y., Cui, H., Ma, H., Chen, J., Liu, N., 2022. Temperature and pressure variations in salt compressed air energy storage (CAES) caverns considering the air flow in the underground wellbore. J. Energy Storage 52, 104846.
Hernandez, D.D., Gençer, E., 2021. Techno-economic analysis of balancing California's power system on a seasonal basis: hydrogen vs. lithium-ion batteries. Appl. Energy 300, 117314.
Jannelli, E., Minutillo, M., Lubrano Lavadera, A., Falcucci, G., 2014. A small-scale CAES (compressed air energy storage) system for stand-alone renewable energy power plant for a radio base station: a sizing-design methodology. Energy 78, 313–322.
Jiang, R., Cai, Z., Peng, K., Yang, M., 2021. Thermo-economic analysis and multi-objective optimization of polygeneration system based on advanced adiabatic compressed air energy storage system. Energy Convers. Manag. 229, 113724.
Kakaç, S., Liu, H., Pramuanjaroenkij, A., 2020. Heat Exchangers: Selection, Rating, and Thermal Design. CRC press.
Kays, W.M., London, A.L., 1984. Compact Heat Exchangers.
King, M., Jain, A., Bhakar, R., Mathur, J., Wang, J., 2021. Overview of current compressed air energy storage projects and analysis of the potential underground storage capacity in India and the UK. Renew. Sustain. Energy Rev. 139, 110705.
Klein, S.A., 1988. TRNSYS-A Transient System Simulation Program. University of Wisconsin-Madison, Engineering Experiment Station Report., 38-12.
Klein, S., Beckman, W., Mitchell, J., Duffie, J., Duffie, N., Freeman, T., et al., 2004. TRNSYS 16–A TRaNsient system simulation program, user manual. Solar Energy. University of Wisconsin-Madison, Laboratory Madison.
Lemmon, E., Huber, M., McLinden, M., 2007. Reference Fluid Thermodynamic and Transport Properties–REFPROP Version 8.0, 23. NIST standard reference database.
Li, C., Chen, D., Li, Y., Li, F., Li, R., Wu, Q., et al., 2022a. Exploring the interaction between renewables and energy storage for zero-carbon electricity systems. Energy 261, 125247.
Li, J.-Q., Li, J.-C.L., Park, K., Kwon, J.-T., 2022b. Investigation on the changes of pressure and temperature in high pressure filling of hydrogen storage tank. Case Stud. Therm. Eng. 37, 102143.
Li, X., Lepour, D., Heymann, F., Maréchal, F., 2023. Electrification and digitalization effects on sectoral energy demand and consumption: a prospective study towards 2050. Energy 279, 127992.
Liu, X., Zhong, L., Wang, J., 2023. The investigation on a hot dry rock compressed air energy storage system. Energy Convers. Manag. 291, 117274.
Logan Jr., E., 2003. Handbook of Turbomachinery. CRC Press.
Luyben, W.L., 2018. Capital cost of compressors for conceptual design. Chemical Engineering and Processing - Process Intensification 126, 206–209.
Ma, L., Zhang, X., Zhang, Z., Wang, Y., Si, Y., Chen, X., et al., 2023. Application of the multi-stage centrifugal compressor 1D loss model in the adiabatic compressed air energy storage. Energy Convers. Manag. 283, 116908.

Maisel, F., Neef, C., Marscheider-Weidemann, F., Nissen, N.F., 2023. A forecast on future raw material demand and recycling potential of lithium-ion batteries in electric vehicles. Resour. Conserv. Recycl. 192, 106920.
Mauro, P.A.W., 2023. Appunti dalle lezioni del corso di tecniche e modelli per la refrigerazione tenute dal Prof. Alfonso William Mauro presso l'Università degli studi di Napoli Federico II.
Mehigan, L., Ó Gallachóir, B., Deane, P., 2022. Batteries and interconnection: competing or complementary roles in the decarbonisation of the European power system? Renew. Energy 196, 1229–1240.
Melideo, D., Baraldi, D., Acosta-Iborra, B., Ortiz Cebolla, R., Moretto, P., 2017. CFD simulations of filling and emptying of hydrogen tanks. Int. J. Hydrogen Energy 42, 7304–7313.
Moran, M.J., Shapiro, H.N., Boettner, D.D., Bailey, M.B., 2014. Fundamentals of Engineering Thermodynamics, eighth ed. Wiley.
Muscio, A., Cossu, M., Morselli, N., Puglia, M., Pedrazzi, S., Allesina, G., 2023. A modified ε-NTU analytical model for the investigation of counter-flow Maisotsenko-based cooling systems. Appl. Therm. Eng. 231, 120944.
Piri, A., Aghanajafi, C., Sohani, A., 2023. Enhancing efficiency of a renewable energy assisted system with adiabatic compressed-air energy storage by application of multiple Kalina recovery cycles. J. Energy Storage 61, 106712.
Politico. U.S. Decides against National Security Tariffs on Rare Earth Magnets from China, Japan, EU, 2024.
Rahbari, H.R., Arabkoohsar, A., 2021. A thorough investigation of the impacts of trigeneration-CAES off-design operation on its thermodynamics, economic and environmental effectiveness. Sustain. Energy Technol. Assessments 44, 101024.
Rane, S., Kovačević, A., Stošić, N., Smith, I., 2021. Analysis of real gas equation of state for CFD modelling of twin screw expanders with R245fa, R290, R1336mzz(Z) and R1233zd(E). Int. J. Refrig. 121, 313–326.
Razmi, A.R., Heydari Afshar, H., Pourahmadiyan, A., Torabi, M., 2021a. Investigation of a combined heat and power (CHP) system based on biomass and compressed air energy storage (CAES). Sustain. Energy Technol. Assessments 46, 101253.
Razmi, A.R., Soltani, M., Ardehali, A., Gharali, K., Dusseault, M.B., Nathwani, J., 2021b. Design, thermodynamic, and wind assessments of a compressed air energy storage (CAES) integrated with two adjacent wind farms: a case study at Abhar and Kahak sites, Iran. Energy 221, 119902.
Reavell - https://www.reavell.com/en/technologies/reavell-reciprocating-compressors.
Salvini, C., Giovannelli, A., 2022. Techno-economic comparison of diabatic CAES with artificial air reservoir and battery energy storage systems. Energy Rep. 8, 601–607.
Sforza, P.M., 2012. Chapter 7 - turbomachinery. In: Sforza, P.M. (Ed.), Theory of Aerospace Propulsion. Butterworth-Heinemann, Boston, pp. 237–305.
Sheng, B., Dong, X., Gong, M., Zhao, Y., 2023. Density and isochoric heat capacity of {x trans-1,3,3,3-Tetrafluoropropene + (1-x) Propane} at temperatures from (285.45 to 349.71) K and pressures up to 10.384 MPa. Int. J. Refrig. 150, 349–356.
Shi, Y., Chen, G., Liu, F., Yue, X., Chen, Z., 2018. Resolving the compositional and structural defects of degraded LiNi x Co y Mn z O2 particles to directly regenerate high-performance lithium-ion battery cathodes. ACS Energy Lett. 3, 1683–1692.
Stewart, M.I., 2014. Chapter three - heat transfer theory. In: Stewart, M.I. (Ed.), Surface Production Operations, third ed. Gulf Professional Publishing, Boston, pp. 39–97.
Tong, Z., Cheng, Z., Tong, S., 2021. A review on the development of compressed air energy storage in China: technical and economic challenges to commercialization. Renew. Sustain. Energy Rev. 135, 110178.
A. Traverso, A.F. Massardo, W. Cazzola, G. Lagorio. Widget-Temp: a novel web-based approach for thermoeconomic analysis and optimization of conventional and innovative cycles. Turbo Expo: Power for Land, Sea, and Air. 2004. pp. 623-631.
Venkataramani, G., Parankusam, P., Ramalingam, V., Wang, J., 2016. A review on compressed air energy storage – a pathway for smart grid and polygeneration. Renew. Sustain. Energy Rev. 62, 895–907.
Vieira, F.S., Balestieri, J.A.P., Matelli, J.A., 2021. Applications of compressed air energy storage in cogeneration systems. Energy 214, 118904.
Volpe, R.D., 2011. Macchine. Liguori.
Wang, L., Wang, P., Cao, Z., Yu, B., Li, W., 2017. Similarity conversion of centrifugal natural gas compressors based on predictor-corrector. Procedia Comput. Sci. 108, 1973–1981.
Wang, J., Ouyang, X., Cheng, L., Peng, S., Wang, Z., Wang, J., 2024. Investigation on adaptability of physical property state equation model for hydrogen-blended natural gas. Int. J. Hydrogen Energy 81, 1256–1277.
Xu, P., Zou, Z., Yao, L., 2021. A unified performance conversion method for similar compressors working with different gases based on polytropic analysis and deep-learning improvement. Energy Convers. Manag. 247, 114747.
Yao, E., Zhong, L., Li, R., Zhao, C., Wu, S., Wang, H., et al., 2023. Enhanced compression heat recovery of coupling thermochemical conversion to trigenerative compressed air energy storage system: systematic sensitivity analysis and multi-objective optimization. J. Energy Storage 68, 107738.
Zhang, N., Cai, R., 2002. Analytical solutions and typical characteristics of part-load performances of single shaft gas turbine and its cogeneration. Energy Convers. Manag. 43, 1323–1337.
Zhang, N., Lin, R., Cai, R.J.J.o.E., 1996. General Formulas for Axial Compressor Performance Estimation, 17, pp. 21–24.
Zhang, L., Liu, L., Zhang, C., He, X., Zhang, Y., Yang, T., 2021. Performance analysis of an adiabatic compressed air energy storage system with a pressure regulation inverter-driven compressor. J. Energy Storage 43, 103197.
Zhang, A., Yin, Z., Wu, Z., Xie, M., Liu, Y., Yu, H., 2023. Investigation of the compressed air energy storage (CAES) system utilizing systems-theoretic process analysis (STPA) towards safe and sustainable energy supply. Renew. Energy 206, 1075–1085.
Zhang, H., Cao, H., Guo, Y., 2024a. The time-varying impact of geopolitical relations on rare earth trade networks: what is the role of China's rare earth export restrictions? Technol. Forecast. Soc. Change 206, 123550.
Zhang, X., Gao, Z., Zhou, B., Guo, H., Xu, Y., Ding, Y., et al., 2024b. Advanced compressed air energy storage systems: fundamentals and applications. Engineering 34, 246–269.
Zhao, L., Zhao, Q., Zhang, J., Zhang, S., He, G., Zhang, M., et al., 2021. Review on studies of the emptying process of compressed hydrogen tanks. Int. J. Hydrogen Energy 46, 22554–22573.
Zhu, J., Cui, X., Ni, W., 2022. Model predictive control based control strategy for battery energy storage system integrated power plant meeting deep load peak shaving demand. J. Energy Storage 46, 103811.